



Published in final edited form as:

J Med Chem. 2017 May 25; 60(10): 4327–4341. doi:10.1021/acs.jmedchem.7b00291.

Exploring the Role of *N*⁶-Substituents in Potent Dual Acting 5'-*C*-Ethyltetrazolyladenosine Derivatives: Synthesis, Binding, Functional Assays, and Antinociceptive Effects in Mice[∇]

Riccardo Petrelli[†], Mirko Scortichini[†], Sonja Kachler[‡], Serena Boccella[§], Carmen Cerchiali^{||}, Ilaria Torquati[†], Fabio Del Bello[†], Daniela Salvemini[⊥], Ettore Novellino^{||}, Livio Luongo[§], Sabatino Maione[§], Kenneth A. Jacobson[#], Antonio Lavecchia^{*||}, Karl-Norbert Klotz[‡], and Loredana Cappellacci^{*†}

[†]School of Pharmacy, Medicinal Chemistry Unit, University of Camerino, Via S. Agostino 1, 62032 Camerino, Italy

[‡]Institut für Pharmakologie and Toxikologie, Universität Würzburg, D-97078 Würzburg, Germany

[§]Section of Pharmacology “L. Donatelli”, Department of Experimental Medicine, University of Campania “L. Vanvitelli”, 80138 Naples, Italy

^{||}Department of Pharmacy, “Drug Discovery” Laboratory, University of Naples Federico II, 80131 Naples, Italy

[⊥]Department of Pharmacology and Physiology, Saint Louis University School of Medicine, St. Louis, Missouri 63104, United States

[#]Laboratory of Bioorganic Chemistry, National Institute of Diabetes and Digestive and Kidney Diseases, National Institutes of Health, Bethesda, Maryland 20892, United States

Abstract

Structural determinants of affinity of *N*⁶-substituted-5'-*C*-(ethyltetrazol-2-yl)adenosine and 2-chloroadenosine derivatives at adenosine receptor (AR) subtypes were studied with binding and molecular modeling. Small *N*⁶-cycloalkyl and 3-halobenzyl groups furnished potent dual acting A₁AR agonists and A₃AR antagonists. **4** was the most potent dual acting human (h) A₁AR agonist (*K*_i = 0.45 nM) and A₃AR antagonist (*K*_i = 0.31 nM) and highly selective versus A_{2A}; **11** and **26** were most potent at both h and rat (r) A₃AR. All *N*⁶-substituted-5'-*C*-(ethyltetrazol-2-

[∇]This work was presented in part at the 6th Joint German–Italian Purine Club Meeting, Purines 2015, Hamburg, Germany, July 2015, and at the 33rd Camerino-Cyprus Symposium. Receptor Chemistry: Reality and Vision, Camerino, Italy, May 2016.

*Corresponding Authors: A.L.: antonio.lavecchia@unina.it; phone, +39-081-678613/623; fax, +39-081-678012. L.C.: loredana.cappellacci@unicam.it; phone, +39-0737-402228; fax, +39-0737-637345.

ORCID

Kenneth A. Jacobson: 0000-0001-8104-1493

Loredana Cappellacci: 0000-0001-8155-7211

Notes

The authors declare the following competing financial interest(s): Daniela Salvemini is cofounder of BioIntervene Inc.

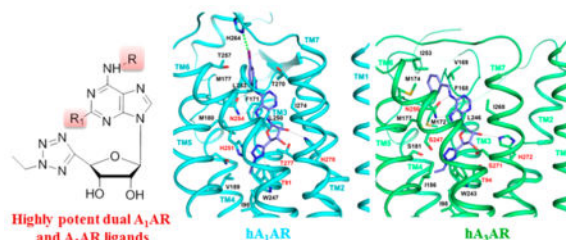
Supporting Information

The Supporting Information is available free of charge on the ACS Publications Web site at DOI: Molecular formula strings (CSV).

The Supporting Information is available free of charge on the ACS Publications website at DOI: 10.1021/acs.jmedchem.7b00291. (CSV)

yl)adenosine derivatives proved to be antagonists at hA₃AR but agonists at the rA₃AR. Analgesia of **11**, **22**, and **26** was evaluated in the mouse formalin test (A₃AR antagonist blocked and A₃AR agonist strongly potentiated). N⁶-Methyl-5'-C-(ethyltetrazol-2-yl)adenosine (**22**) was most potent, inhibiting both phases, as observed combining A₁AR and A₃AR agonists. This study demonstrated for the first time the advantages of a single molecule activating two AR pathways both leading to benefit in this acute pain model.

Graphical Abstract



INTRODUCTION

Adenosine, the natural ligand of P1 receptors, is implicated in the control of many physiological and pathological conditions such as inflammation, pain, and cardiovascular and central nervous system (CNS) diseases.^{1,2} P1 receptors belong to the large family of G-protein-coupled receptors (GPCRs) and are represented by four subtypes: A₁, A_{2A}, A_{2B}, and A₃ adenosine receptors (ARs).

Owing to the wide distribution of AR subtypes in virtually all tissues, avoiding side effects has a high priority in the development of selective AR ligands as therapeutic agents. However, designing a single drug molecule able to specifically interact with several targets simultaneously is becoming a major trend in drug discovery.^{3,4} A multitarget drug may display an improved therapeutic efficacy compared to a highly selective one. In fact, multitarget activities may potentiate the effect of treatment either additively or synergistically. Moreover, a multitarget drug has the advantage of following only one pharmacokinetic and metabolic pattern, thus overcoming the limits of combination therapy.

In the AR field, several examples of dual acting ligands have been reported. A dual A_{2A}AR agonist and A₃AR antagonist has been investigated by Glaxo as an anti-inflammatory agent.⁵ Hou et al. reported dual acting hA_{2A} agonists and hA₃AR antagonists potentially useful in asthma and inflammatory diseases.⁶

Very recently, we reported the first highly potent dual acting hA₁AR agonists and hA₃AR antagonists potentially useful in the treatment of glaucoma and epilepsy.⁷ Combining a 5'-Cethyltetrazol-2-yl group with the appropriate N⁶-substitution in adenosine derivatives led to an increased affinity versus both hA₁AR and hA₃AR, reaching subnanomolar values, while remaining agonists at hA₁ and antagonists at hA₃AR.

The aim of this study was to extend the series of 5'-C-(ethyltetrazol-2-yl)adenosine and 2-chloroadenosine derivatives, modifying the substituent in the N⁶-position of the adenine ring

(compounds **1–17**). Moreover, it is well-known that A₃AR represents the AR subtype with high species differences for both affinity and efficacy.⁸ For this reason we assayed the affinity and efficacy of some selected compounds also at the rat (r) A₃AR.

Salvemini and colleagues and others have reported that highly selective A₃ agonists reduce neuropathic pain in various models of neuropathic pain states including bone cancer pain, and some A₃AR agonists are in preclinical studies for the treatment of these diseases.^{9–14} Our previous work demonstrated that also potent and selective A₁AR agonists are effective in pain conditions.^{15–18} Therefore, combining the analgesic effects of both A₁ and A₃AR agonists in only one molecule might be highly advantageous in terms of reducing side effects and synergizing the antinociceptive activities.

RESULTS AND DISCUSSION

Chemistry

Compounds **1–17** were synthesized by reacting 2-(6-chloro-9*H*-purin-9-yl)-5-(2-ethyl-2*H*-tetrazol-5-yl)-tetrahydrofuran-3,4-diyl diacetate (**18**) or 2-(2,6-dichloro-9*H*-purin-9-yl)-5-(2-ethyl-2*H*-tetrazol-5-yl)tetrahydrofuran-3,4-diyl diacetate (**19**),⁷ with cycloalkyl, arylalkyl, or heteroaryl amines followed by the sugar deprotection in basic conditions (Scheme 1). Intermediates **18**, **19**, and reference compounds **20–26** (see Table 1) were synthesized as previously reported.⁷

Binding Affinity

Compounds **1–17** were tested for affinity for the human recombinant ARs, stably transfected into Chinese hamster ovary (CHO) cells, utilizing radioligand binding assays (A₁, A_{2A}, and A₃) or an adenylyl cyclase activity assay (A_{2B}) (Tables 1 and 2).¹⁹ Selected compounds were also tested at the recombinant rA₃AR, stably transfected into CHO cells utilizing radioligand binding assays, and the results are reported in Table 3.

As shown in Table 1, the introduction of a cyclopropyl or a cyclopropylmethyl group in N⁶-position furnished very potent dual hA₁AR agonists and hA₃AR antagonists (**1–4**) with K_i values at both receptor subtypes in the subnanomolar range (K_i = 0.44–0.86 nM at A₁AR; K_i = 0.31–0.87 nM at A₃AR). Substitution with a heteroaryl group (compounds **5–8**) reduced the affinity in the low nanomolar range at both hA₁ (K_i = 3.53–10.7 nM) and hA₃ (K_i = 1.31–4.85 nM) ARs. The reduction of affinity was more evident at hA₁AR than at hA₃AR. The effect on A₁ and A₃ AR affinities of a halogen at 3-position of N⁶-benzyl-5'-*C*-(ethyltetrazol-2-yl)adenosine derivatives was also investigated.

Affinities at hA₁AR of 5'-*C*-ethyltetrazol-2-yl-adenosine derivatives **9–15** increased with the size of the halogen. In fact, the rank order was 3-iodo-benzyl (**15**, K_i = 0.77) > 3-bromobenzyl (**13**, K_i = 0.95 nM) > 3-chlorobenzyl (**11**, K_i = 1.41 nM) > 3-fluorobenzyl (**9**, K_i = 3.73 nM). At hA₃AR, except for 3-fluorobenzyl derivative **9** (K_i = 1.20 nM), 3-chlorobenzyl (**11**, K_i = 0.39 nM), 3-bromobenzyl (**13**, K_i = 0.39 nM), and 3-iodobenzyl (**15**, K_i = 0.53 nM) derivatives were almost equipotent, showing subnanomolar affinities. The same results were reported by Jacobson et al. in the 4'-truncated N⁶-substituted-(*N*)-methanocarbaadenosine derivatives.²⁰ It is surprising to note that the corresponding 2-chloro

derivatives (compounds **10**, **12**, **14**, and **26**,⁷ respectively) were less active at hA₁AR (K_i = 2.71–6.04 nM), while at hA₃AR their affinities remained in the subnanomolar range (K_i = 0.34–0.58 nM) and marginally increased for the 3-fluorobenzyl-2-chloroadenosine derivative **10** (K_i = 0.81 nM). It should be underlined that except for 3-fluorobenzyladenosine derivative **9**, all *N*⁶-cycloalkyl and *N*⁶-3-halobenzyl derivatives (compounds **1–4** and **9–15**, respectively) showed subnanomolar affinity at hA₃AR. The most potent 3-halobenzyl derivatives at A₁AR were the 3-bromobenzyl and 3-iodobenzyl derivatives (**13** and **15**), with K_i values in the subnanomolar range (K_i = 0.95 and 0.77 nM, respectively). With reduction of the size of the halogen, the affinity at A₁AR decreased from 0.77 (3-iodo-, **15**) to 6.04 nM (3-fluoro-, **10**). However, an *N*⁶-3-fluorobenzyl substituent increased the A_{2A}/A₃ selectivity and compound **10** was the most selective A_{2A}/A₃ ligand in the 3-halobenzyl series (A_{2A}/A₃ = 299, Table 4).

Unexpectedly, the introduction of a chlorine at 2-position of the purine ring of this series did not improve the A₁AR affinity. The 2-chloro substitution also did not influence the affinity at A₃AR but led to a 4.8-fold increase of the A_{2A}/A₃ selectivity (e.g., compound **9**, A_{2A}/A₃ selectivity = 62; compound **10** = 299).

The 2-fluoro-4-chlorobenzyl substituent in *N*⁶-position (compounds **16** and **17**) reduced the affinity at both A₁AR (K_i = 4.28 and 17.6 nM) and A₃AR (K_i = 4.67 and 5.17 nM) with respect to the 3-halobenzyl derivatives and also compared to previously reported 2-fluoro-4-chlorophenyl derivatives **24** and **25** (K_i = 0.43 and 1.67 nM at A₁AR and 2.61 and 4.71 nM at A₃AR, respectively).⁷ As reported in our previous work,⁷ upon replacing the 5'-hydroxymethyl group in adenosine derivatives with the 5'-*C*-ethyltetrazol-2-yl, very high affinities at both hA₁ and hA₃ ARs were maintained, even with a small cycloalkyl group at the *N*⁶-position. *N*⁶-Cyclopropyl- and *N*⁶-cyclopropylmethyl-5'-*C*-ethyltetrazol-2-yladenosine and 2-chloroadenosine derivatives (compounds **1–4**) emerged as the most potent dual acting hA₁AR agonists (K_i = 0.44–0.86 nM) and hA₃AR antagonists (K_i = 0.31–0.87 nM) of the series and were highly selective versus A_{2A}. In particular, compound **4** (K_i = 0.45 and 0.31 nM at hA₁ and hA₃AR, respectively) was 725-fold A₁ selective versus A_{2A} and 1097-fold A₃ selective versus A_{2A} and was therefore the most potent and selective compound of the series. Also, compound **2** was highly selective for A₁ (510-fold over A_{2A}) and A₃ (596-fold over A_{2A}). It is interesting to note that in all compounds of the series the 2-chloro derivatives were less potent at A_{2A} than the 2-unsubstituted counterparts (e.g., **4** vs **3**, **10** vs **9**, **12** vs **11**, etc.). Moreover, as we previously reported,⁷ the A_{2A}AR does not seem to tolerate alkyl and cycloalkyl groups at the *N*⁶-position (**1–4**, A_{2A} K_i = 112–329 nM) but better tolerates 3-halobenzyl substituents (**9–15**, A_{2A} K_i = 16.8–242 nM).

Owing to the species differences of affinity and efficacy at A₃AR, some selected compounds were also tested at rA₃A. K_i values of selected compounds at hA₃AR and rA₃AR are compared (Table 3). In general, all compounds showed weaker binding affinities at rA₃AR than at hA₃AR as previously reported also by Jacobson et al. in a series of truncated *N*⁶-substituted-(*N*)-methanocarbaadenosine derivatives.²⁰ Surprisingly, at rA₃AR all tested compounds switched from antagonists to full agonists. It is interesting to note that 3-halobenzyl derivatives **9**, **11**, **13**, **15**, and **26** emerged as the most potent compounds at rA₃AR, whereas compounds **1** and **3** were 76- and 114-fold less potent at rA₃AR than at

hA₃AR (rA₃AR K_i = 66.0 and 65.2 nM, respectively; hA₃AR K_i = 0.87 and 0.57 nM, respectively). The most potent compounds at both hA₃AR and rA₃AR were the 3-iodobenzyl-2-chloroadenosine derivative **26** (K_i rA₃AR = 2.53 nM; hA₃AR = 0.59 nM; rA₃AR/hA₃AR = 4.3) and the 3-chlorobenzyladenosine derivative **11** (K_i rA₃AR = 2.69 nM; hA₃AR = 0.39 nM; rA₃AR/hA₃AR = 6.9). The highest differences were seen with a *N*⁶-methyl substituent: compounds **22** and **23** were 1000- and 1400-fold less potent at rA₃AR than at hA₃AR, respectively.

Adenylyl Cyclase Activity

All novel compounds were tested in a functional A_{2B}AR assay and some showed a moderate potency in stimulation of adenylyl cyclase activity (Table 2). The most potent compound was **1** (EC₅₀ = 222 nM), while the least potent was **17** (EC₅₀ > 30 000 nM). It is noteworthy that **1**, **3**, and **9** behaved as partial A_{2B}AR agonists, whereas all other compounds acted as full agonists (Table 2). All compounds were additionally tested for their functional effects on human A₁, A_{2A}, and A₃ ARs by determination of adenylyl cyclase activity. As expected, all tested compounds were found to be agonists at A₁ and A_{2A} ARs, whereas they were antagonists at the A₃ subtype (Table 2). Interestingly, only compound **15** was found to be a partial agonist at A₁AR. Compounds **1–4** showed the best EC₅₀ values of the series at hA₁AR (7.21–7.73 nM), whereas the most potent hA₃AR antagonists **3**, **11**, **13**, and **15** displayed EC₅₀ values at hA₃AR ranging from 2.07 to 3.53 nM, presenting as the most potent hA₃AR antagonists of the series and also compared to the 5'-C-tetrazol-2-yladenosine derivatives previously published by us.⁷ Among the tested compounds, the best EC₅₀ values at A_{2A}AR were displayed by **11** (6.71 nM), **13** (4.46 nM), and **15** (2.87 nM). Some selected compounds were also tested at rA₃AR in a cAMP functional assay and turned out to be full A₃AR agonists.

Molecular Modeling

The 5'-C-(ethyltetrazol-2-yl)-adenosine derivatives acting dually at hA₁AR and hA₃AR, i.e., **9** (A₁, K_i = 3.73 nM), **11** (A₁, K_i = 1.41 nM), **13** (A₁, K_i = 0.95 nM), and **15** (A₁, K_i = 0.77 nM), exhibited increased binding affinity at the hA₁AR upon changing the substituent on the *N*⁶-benzyl moiety from F to Cl, Br, and I, and the same derivatives were almost equipotent at hA₃AR (**9**, A₃, K_i = 1.20 nM; **11**, A₃, K_i = 0.39 nM; **13**, A₃, K_i = 0.39 nM; **15**, A₃, K_i = 0.53 nM). To rationalize the observed variations in the hA₁AR and hA₃AR binding affinities among these compounds, molecular docking calculations were carried out using homology models of the hA₁- and hA₃ARs. In particular, two previously reported models were used: a hA₁AR model entirely based on an agonist-bound hA_{2A}AR crystal structure (PDB code 3QAK)^{21,22} and a hA₃AR model based on a hybrid A_{2A}AR β_2 adrenergic receptor template, where TM2 is shifted outward from the binding site.^{23,24}

Docking was carried out using the GOLD Suite 5.4.1 docking package²⁵ in combination with the ChemPLP²⁶ scoring function (rescoring with ChemScore).²⁷

In docking of selected compounds in the present series, a common binding mode was obtained in both the hA₁AR and hA₃AR models, and this mode featured all the key interactions found to anchor the adenine and ribose moieties of similar derivatives.⁷ As an

example, Figure 1 shows the docking poses of compound **15**, which displayed high affinity at the two receptors.

The side chain at position 6.55 (using standard notation;²⁸ N254 in the hA₁AR and N250 in the hA₃AR) strongly interacted with the two compounds through two H-bonds involving the 6-amino group and the adenine N7 atom. Moreover, the adenine ring was engaged in aromatic π - π stacking with a conserved phenylalanine in EL2 (F171 in the hA₁AR and F168 in the hA₃AR) and strong hydrophobic contacts with leucine 6.51 (L250 in hA₁AR and L246 in hA₃AR) and isoleucine 7.39 (I274 in the hA₁AR and I268 in the hA₃AR).

The 3'- and 2'-OH groups of the ribose ring formed H-bonds with the side chains at positions 7.42 (T277 in hA₁AR and S271 in hA₃AR) and 7.43 (H278 in hA₁AR and H272 in hA₃AR), respectively. The 5'-C-tetrazole ring was stabilized by two strong H-bonds with T91^{3.36} and H251^{6.52} side chains in the hA₁AR, whereas it was not able to interact either with T94^{3.36} or with S247^{6.52} in the hA₃AR. The residue at position 3.36 is conserved among all four AR subtypes, while the one at position 6.52 is conserved in hA₁-, hA_{2A}-, and hA_{2B}ARs but is substituted with a smaller serine in the hA₃AR. These polar amino acids at TMs 3 and 7 play key roles in the binding of the hydrophilic ribose moiety of nucleoside agonists and are considered to be important for receptor activation.^{22,29} Thus, the missing interaction with T94^{3.36} and/or S247^{6.52} was considered the reason for the low efficacy profile of these 5'-C-tetrazoleethyl nucleosides at the hA₃AR. In fact, even though no mutagenesis data are available for position 3.36 at the hA₃ subtype, previous mutagenesis studies have shown the importance of this threonine in agonist but not antagonist binding at the hA₁ and hA_{2A} subtypes.^{30,31} Therefore, interaction of ligands with T^{3.36} might be crucial to lock the 5'-ribose moiety in an optimal conformation to strongly interact with residues at positions 7.42 and 7.43 in order to pull TM7 toward TM3 to efficiently activate the receptor.

As shown in Figure 1A, the N⁶-3-iodobenzyl substituent of **15** perfectly fit in a hydrophobic pocket, located between TM6 and TM7 of hA₁AR and delimited by residues L253^{6.54}, T257^{6.58}, T270^{7.35} and at the bottom by L250^{6.51}. It is to be noted that the iodine, bromine, and chlorine atoms of adenosine derivatives **15**, **13**, and **11** appeared perfectly poised for halogen bonding with the N⁶ atom of H264^{6.66}. This interaction is characterized by the requirement for nearly colinear alignment of the halogen bond donor C-X (where X = F, Cl, Br, I) with the halogen bond acceptor atom at a distance less than the van der Waals (vdW) distance, thus allowing the acceptor atom to orient its electron density into the σ -hole, which corresponds to the σ^* -orbital of the C-X bond (Figure 2). Typically, the distance between the halogen atom and the nitrogen atom (X...N) is equal to or less than the sum of their radii (3.02 Å for F...N; 3.30 Å for Cl...N; 3.40 Å for Br...N; 3.53 Å for I...N),^{32,33} while the mean values for the C-X...N angle are 154.6° for Cl, 164.1° for Br, 171.4° for I.³⁴ The complex of 3-Cl-benzyl derivative **11** showed a Cl...N distance of 3.0 Å (91% sum of vdW radii) and a C-Cl...N angle of 161° (Figure 2B). In the complex of the 3-Br-benzyl derivative **13**, the Br...N distance was 3.1 Å (88% sum of vdW radii) and the C-Br...N angle was 164° (Figure 2C). With an I...N distance of 3.0 Å (85% sum of vdW radii) and a C-I...N angle of 161° (Figure 2D), the 3-I-benzyl derivative **15** displayed the closest contact of the halide to the H264^{6.66} nitrogen atom. These intermolecular distances are in very good agreement with

quantum mechanically calculated minimum energy separations (3.0–3.1 Å) in model systems of a histidine side chain interacting with halogen-substituted phenyls.³⁵ The predicted gain in interaction energy by approximately 1 kcal/mol from Cl to Br to I each correlates qualitatively with the observed increase in binding affinity (Table 1). In sharp contrast, the F atom in compound **9** bound to hA₁AR was located at an F···N distance of 3.8 Å and a C–I···N angle of 125° (Figure 2A), indicative of an unfavorable interaction when organofluorine pointed at the N atom of H264^{6,66}. This is reflected in the approximately 5-fold lower K_i value for binding to the hA₁AR.

On the other hand, in the binding pose of derivatives **9–15** at the hA₃AR, the *N*⁶-3-halobenzyl substituents were in proximity of a small, secondary (side) pocket delimited by TM5, TM6, and EL2 (Figure 1C) and established strong hydrophobic interactions with residues V169^{EL2}, M172^{EL2}, M174^{5,35}, M177^{5,38}, and I253^{6,58}. A specific S··· π interaction was observed between the residue M174 and the *N*⁶-3-halobenzyl ring of **9–15**. The sulfur atom of M174 was 3.6 and 3.7 Å from the bridgehead carbons of the 3-halobenzyl ring in the bound ligands.³⁶ The good fit of these substituents with this region can explain the very high affinity of such compounds at the hA₃AR. As reported in Table 1, the binding affinity correlated well with the increasing lipophilicity of the halogen substituent at position 3 of the benzyl ring (K_i values from 1.20 nM for the 3-F-benzyl derivative **9** to 0.532 nM for 3-I-benzyl derivative **15**). The size of the halogen could also contribute to the effect since the larger iodine led to a 0.7-fold decrease of the binding affinity in comparison to the smaller bromine and chlorine.

To understand the gain of A_{2A}AR affinity of the *N*⁶-(3-halobenzyl) derivatives (compounds **9–15**) compared to the *N*⁶-alkyl or cycloalkyl ones (compounds **1–4**), **15** was docked into the binding site of the A_{2A}AR crystal structure. In the docked poses of compound **15** inside the A_{2A}AR, the benzyl ring formed an edge-to-face π -stacking interaction with the Tyr271^{7,36} aromatic ring, whereas the 3-Cl atom was within proper distance to make halogen bond interactions to the negatively charged carboxylate group of Glu169^{EL2}. The absence of these interactions in the **1**/A_{2A}AR complex rationalized the diminished A_{2A}AR affinity of *N*⁶-alkyl or cycloalkyl derivatives **1–4**.

Formalin Test

Antinociceptive Effect—We have evaluated the potential analgesic activity of some 5'-*C*-tetrazolyl-*N*⁶-adenosine derivatives using the formalin test. Formalin injection induces a biphasic stereotypical nocifensive behavior.³⁷ Nociceptive responses are divided into an early, short lasting first phase (0–7 min) caused by a primary afferent discharge produced by the stimulus, followed by a quiescent period and then a second, prolonged phase (15–60 min) of tonic pain. Formalin tests were performed on compounds **11**, **22**, and **26** (Figures 3 and 4). Surprisingly, compound **26** at the highest dose tested (1 mg/kg, ip) was inactive (Figure 3B), while systemic administration of **11** (0.5–1.0 mg/kg, ip), 10 min before formalin (Figure 3A), reduced the late nociceptive behavior induced by formalin in a dose-dependent manner ($P < 0.005$). The most potent compound was compound **22**. In fact, systemic administration of **22** at 0.3 mg/kg, ip, 10 min before formalin (Figure 4A) reduced the late nociceptive behavior induced by formalin, and this effect was dose-dependent. Our

previous work demonstrated that systemic 2-chloro-2'-*C*-methyl-*N*⁶-cyclopentyladenosine (**27**, 2'-MeCCPA, 2.5–5 mg/kg, ip)¹⁵ and 5'-chloro-5'-deoxy-*N*⁶-(±)-*endo*-norborm-2-yl)adenosine (**28**, 5'Cl15'd-(±)-ENBA, 1–2 mg/kg, ip),¹⁶ two potent and selective A₁AR agonists, also inhibited the second phase of formalin-induced hyperalgesia in a dose-dependent manner, and this effect was blocked by 8-cyclopentyl-1,3-dipropylxanthine (**29**, DPCPX, 3 mg/kg, ip), a selective A₁AR antagonist.

In order to prove that the strong analgesic effect of **22** depends also on its A₃ agonistic activity, an experiment with 1,4-dihydro-2-methyl-6-phenyl-4-(phenylethynyl)-3,5-pyridine-dicarboxylic acid 3-ethyl-5-[(3-nitrophenyl)methyl] ester (**30**, MRS1334),³⁸ a selective A₃ receptor antagonist, was carried out. As shown in Figure 4B the antinociceptive effect of **22** (0.5 mg/kg, ip) was reverted by **30** (2 mg/kg, ip), demonstrating that in **22** both the A₁ and A₃ agonistic effects contributed to the analgesic behavior. This result was further confirmed by an experiment in which a combination of **28** (1 mg/kg, ip) and 2-chloro-*N*⁶-(3-iodobenzyl)-5'-*N*-methylcarboxamidoadenosine (**31**, 2Cl-IBMECA, 1 mg/kg, ip) was assayed in formalin test in mice. As shown in Figures 5 and 6 the combination of **28**, the most selective A₁ agonist so far known (hA₁AR vs hA₃AR ~2600-fold¹⁶ and mouse A₁AR vs A₃AR ~10 000-fold³⁹), and a selective A₃ agonist (**31**) showed greater effects when combined in reducing both the first and the second phases of formalin test.

Moreover, systemic administration of the combination of **22** (0.3 mg/kg ip) and **31** (1 mg/kg ip), 10 min before formalin injection, completely erased the second phase and reduced the first phase of formalin-induced nociceptive behavior ($P < 0.005$) (Figure 7). A₁ agonists can at high doses reduce the early phase,¹⁶ whereas A₃ agonists do not affect the first phase.¹² However, in this study we showed that molecule with hybrid mechanism of action (A₁/A₃ agonist) or the combination of A₁AR and A₃AR agonists, co-injected simultaneously, can reduce both the early and the late phases associated with the formalin injection. This effect can be due to the A₁ component. Interestingly, also subthreshold doses of both A₁ and A₃ agonists (0.5 mg/kg ip, Figure 6), which did not reduce either the first or the second phase of formalin per se, decreased both early and late phases when co-injected in this model. This effect needs further investigation to better understand how A₁ and A₃ARs can cooperate and/or how A₃AR stimulation could sensitize the A₁AR, in turn making it more able to reduce the first phase at low doses.

The loss of antinociceptive effect displayed by **26** compared to the good analgesic effect of **11** is quite surprising because these compounds displayed similar affinity and efficacy profiles at both human and rat A₁ARs. Furthermore, **26** could have more favorable blood–brain transport characteristics owing to its higher lipophilicity (log $P = 4.06$) vs **11** (log $P = 2.57$). Further studies are needed to verify if the loss of activity of **26** is due to some metabolic instability.

CONCLUSIONS

This study reports for the first time that potent dual acting *N*⁶-substituted-5'-*C*-(ethyltetrazol-2-yl)adenosine and 2-chloroadenosine derivatives showed strikingly different efficacy at human and rat A₃ARs, acting as antagonists at hA₃A and as agonists at rA₃AR.

The combination of a 5'-*C*-ethyltetrazol-2-yl moiety with a small cycloalkyl or 3-halobenzyl group at *N*⁶-position in adenosine derivatives provided very potent dual A₁ and A₃ ligands at both human and rat A₁ and A₃ARs. This novel series allowed us to discover *N*⁶-cyclopropylmethyl-5'-*C*-(ethyltetrazol-2-yl)-2-chloroadenosine (**4**), a very potent dual A₁/A₃ agonist in rat and A₁ agonist/A₃ antagonist in human, confirming the concept that the "cyclopropyl fragment" is a versatile player which confers high affinity also in this class of AR ligands. The most potent antinocifensive activity was obtained with compound **22**, which at 0.5 mg/kg reduced both the first and the second phases of formalin test. A combination of **22** (0.3 mg/kg) with A₃AR agonist **31** (1 mg/kg) reduced completely the nocifensive behavior in both the first and the second phases of formalin test.

In conclusion, this study demonstrates that a combination of an A₁ agonist and an A₃AR agonist shows a highly potent analgesic activity. Therefore, combining both A₁ and A₃AR agonistic activity in one single molecule, such as the 5'-*C*-tetrazolyl-*N*⁶-substituted adenosine derivatives, could be beneficial for the treatment of pain. This series of 5'-*C*-(ethyltetrazol-2-yl)adenosine derivatives may open the field to the research of more active and less toxic analgesic drugs in the treatment of neuropathic pain. Moreover, they represent very useful pharmacological tools for in vivo studies in order to investigate the advantages of dual acting A₁ and A₃AR agonists in cardio- and neuroprotection. Finally, due to their different efficacy at A₃AR in two species, further studies are needed in order to identify an animal model that reproduces the efficacy shown by this series of compounds in humans, i.e., A₁AR agonism and A₃AR antagonism. This animal model will allow us to study the advantages of a single molecule with one pharmacokinetic profile, activating one signaling pathway while blocking another one, both leading to beneficial effects for the treatment of diseases such as glaucoma and epilepsy.

EXPERIMENTAL SECTION

Chemical Synthesis. Materials and Instrumentation

All reagents and solvents were purchased from Sigma-Aldrich Chemical Co, were analytical grade, and were used as received. Thin layer chromatography (TLC) was run on silica gel 60 F254 plates; silica gel 60 (70–230 mesh Merck and 200–400 mesh, Merck) for column chromatography was used. Preparative thin layer chromatography was run on silica gel GF (20 cm × 20 cm, 1000 μm, Analtech). The final compounds were characterized by ¹H NMR, ¹³C NMR, MS, and elemental analyses. ¹H NMR and ¹³C NMR spectra were recorded on 400 MHz NMR spectrometer (Varian Mercury AS400 instrument). The chemical shift values are expressed in δ values (ppm), and coupling constants (*J*) are in hertz; tetramethylsilane (TMS) was used as an internal standard. Proton chemical data are reported as follows: chemical shift, multiplicity (s = singlet, d = doublet, dd = doublet of doublets, pd = pseudo doublet, t = triplet, dt = doublet of triplets, pt = pseudo triplet, q = quartet, dq = doublet of quartets, pq = pseudo quartet, m = multiplet, brs = broad singlet) coupling constant(s), integration. The presence of all exchangeable protons was confirmed by addition of D₂O. The purity of final compounds was checked using an Agilent 1100 series instrument equipped with Gemini-NX, 5 μm C-18 100 Å, 250 mm × 4.6 mm. Mobile phase consisted of a mixture of water/methanol (95:5) at a flow rate of 1 mL/min. Peaks

were detected by UV adsorption with a diode array detector (DAD) at 230, 254 and, 280 nm. All derivatives tested for biological activity showed 96% purity by HPLC analysis (area % purity was detected at 210 or 254 nm). Mass spectra were recorded on an HP 1100 series instrument. All measurements were performed in the positive ion mode using atmospheric pressure electrospray ionization (API-ESI). Elemental analyses (C, H, and N) were determined on ThermoFisher Scientific FLASH 2000 CHNS analyzer and are within 0.4% of theoretical values.

General Procedure for the Amination of 18 or 19 into Compounds 1–17

To a stirred solution of (2*R*,3*R*,4*R*,5*R*)-2-(6-chloro-9*H*-purin-9-yl)-5-(2-ethyl-2*H*-tetrazol-5-yl)tetrahydrofuran-3,4-diyl diacetate (**18**)⁷ (1.0 mmol) or (2*R*,3*R*,4*R*,5*R*)-2-(2,6-dichloro-9*H*-purin-9-yl)-5-(2-ethyl-2*H*-tetrazol-5-yl)tetrahydrofuran-3,4-diyl diacetate (**19**)⁷ (1.0 mmol) in absolute ethanol (20 mL) and TEA (3.0 mmol) only in the case of compounds **15–17**, the appropriate ammine (1.6 mmol) was added. The reaction mixture was refluxed for the time reported below and concentrated in vacuo. The residue was dissolved in methanolic ammonia (10 mL) and stirred at room temperature overnight. The solution was evaporated to dryness, and the residue was purified by chromatography on a silica gel column.

(2*R*,3*S*,4*R*,5*R*)-2-(6-(Cyclopropylamino)-9*H*-purin-9-yl)-5-(2-ethyl-2*H*-tetrazol-5-yl)tetrahydrofuran-3,4-diol (1)—Reaction of **18** with cyclopropylamine at reflux for 5 h followed by deprotection and chromatography on a silica gel column (CHCl₃–MeOH, 95:5) gave **1** as a white solid (45% yield). ¹H NMR (400 MHz, DMSO): δ 0.57–0.61 (m, 2H), 0.68–0.75 (m, 2H), 1.50 (t, *J* = 7.3 Hz, 3H), 2.90–3.10 (m, 1H), 4.62–4.57 (m, 1H), 4.70 (q, *J* = 7.2 Hz, 2H), 4.76–4.84 (m, 1H), 5.20 (d, *J* = 4.7 Hz, 1H), 5.75 (d, *J* = 5.9 Hz, 1H), 5.82 (d, *J* = 5.9 Hz, 1H), 6.10 (d, *J* = 5.1 Hz, 1H), 7.90 (brs, 1H), 8.20 (s, 1H), 8.40 (s, 1H). ¹³C NMR (DMSO-*d*₆): 7.71, 7.92, 14.33, 26.45, 48.32, 73.62, 73.93, 76.48, 88.01, 118.54, 139.78, 149.22, 153.01, 156.28, 164.06 ppm. MS (API-ESI): *m/z* 374.17 [M + H]⁺. Anal. Calcd for C₁₅H₁₉N₉O₃: C, 48.25; H, 5.13; N, 33.76. Found: C, 48.26; H, 3.12; N, 33.75.

(2*R*,3*R*,4*S*,5*R*)-2-(2-Chloro-6-(cyclopropylamino)-9*H*-purin-9-yl)-5-(2-ethyl-2*H*-tetrazol-5-yl)tetrahydrofuran-3,4-diol (2)—Reaction of **19** with cyclopropylamine at reflux for 4 h followed by deprotection and chromatography on a silica gel column (CHCl₃–MeOH, 95:5) gave **2** as a white solid (61% yield). ¹H NMR (DMSO-*d*₆): δ 0.60 (s, 2H), 0.70 (s, 2H), 1.50 (t, *J* = 7.2 Hz, 3H), 2.95 (brs, 1H), 4.55 (d, *J* = 5.1 Hz, 1H), 4.71 (q, *J* = 7.2 Hz, 2H), 4.78 (q, *J* = 5.3 Hz, 1H), 5.20 (d, *J* = 3.8 Hz, 1H), 5.80 (d, *J* = 5.5 Hz, 1H), 5.85 (d, *J* = 5.9 Hz, 1H), 6.05 (d, *J* = 5.1 Hz, 1H), 8.41 (s, 1H), 8.50 (brs, 1H). ¹³C NMR (DMSO-*d*₆): 7.74, 7.91, 14.26, 26.34, 48.73, 73.02, 73.87, 75.91, 88.57, 119.02, 140.11, 149.57, 153.21, 155.93, 164.28 ppm. MS (API-ESI): *m/z* 408.12 [M + H]⁺. Anal. Calcd for C₁₅H₁₈ClN₉O₃: C, 44.18; H, 4.45; N, 30.91. Found: C, 44.17; H, 4.46; N, 30.92.

(2*R*,3*S*,4*R*,5*R*)-2-(6-((Cyclopropylmethyl)amino)-9*H*-purin-9-yl)-5-(2-ethyl-2*H*-tetrazol-5-yl)tetrahydrofuran-3,4-diol (3)—Reaction of **18** with cyclopropanemethylamine at reflux for 6 h followed by deprotection and chromatography on a silica gel column (CHCl₃–MeOH, 97:3) gave **3** as a white solid (89% yield). ¹H NMR

(DMSO- d_6): δ 0.21–0.27 (m, 2H), 0.36–0.41 (m, 2H), 1.08–1.12 (m, 1H), 1.52 (t, J = 7.5 Hz, 3H), 3.31–3.42 (m, 2H), 4.57–4.61 (m, 1H), 4.71 (q, J = 7.2 Hz, 2H), 4.82 (q, J = 4.9 Hz, 1H), 5.18 (d, J = 4.3 Hz, 1H), 5.75 (d, J = 5.9 Hz, 1H), 5.82 (d, J = 5.9 Hz, 1H), 6.11 (d, J = 4.7 Hz, 1H), 7.91 (brs, 1H), 8.18 (s, 1H), 8.38 (s, 1H). ^{13}C NMR (DMSO- d_6): 7.22, 7.31, 10.94, 14.46, 48.81, 60.22, 73.32, 74.01, 75.33, 88.62, 118.69, 140.57, 149.84, 152.92, 155.43, 164.31 ppm. MS (API-ESI): m/z 388.18 $[\text{M} + \text{H}]^+$. Anal. Calcd for $\text{C}_{16}\text{H}_{21}\text{N}_9\text{O}_3$: C, 49.61; H, 5.46; N, 32.54. Found: C, 49.59; H, 5.45; N, 32.55.

(2R,3R,4S,5R)-2-(2-Chloro-6-((cyclopropylmethyl)amino)-9H-purin-9-yl)-5-(2-ethyl-2H-tetrazol-5-yl)tetrahydrofuran-3,4-diol (4)—Reaction of **19** with

cyclopropylmethylamine at reflux for 4 h followed by deprotection and chromatography on a silica gel column (CHCl_3 –MeOH, 97:3) gave **4** as a white solid (57% yield). ^1H NMR (DMSO- d_6): δ 0.25 (pq, J = 4.7 Hz, 2H), 0.38–0.43 (m, 2H), 1.05–1.12 (m, 1H), 1.50 (t, J = 7.2 Hz, 3H), 3.21–3.29 (m, 2H), 4.51–4.58 (m, 1H), 4.72 (q, J = 7.4 Hz, 2H), 4.75–4.93 (m, 1H), 5.21 (d, J = 4.2 Hz, 1H), 5.81 (d, J = 5.9 Hz, 1H), 5.85 (d, J = 5.9 Hz, 1H), 6.03 (d, J = 4.7 Hz, 1H), 8.41 (s, 1H), 8.48 (brs, 1H). ^{13}C NMR (DMSO- d_6): 7.22, 7.29, 10.65, 14.57, 48.32, 60.43, 73.24, 73.88, 75.18, 89.01, 119.03, 140.63, 149.57, 153.05, 155.82, 164.41 ppm. MS (API-ESI): m/z 422.14 $[\text{M} + \text{H}]^+$. Anal. Calcd for $\text{C}_{16}\text{H}_{20}\text{ClN}_9\text{O}_3$: C, 45.56; H, 4.78; N, 29.88. Found: C, 45.57; H, 4.77; N, 29.86.

(2R,3S,4R,5R)-2-(2-Ethyl-2H-tetrazol-5-yl)-5-(6-((furan-2-ylmethyl)amino)-9H-purin-9-yl)tetrahydrofuran-3,4-diol (5)—Reaction of **18** with furfurylamine at reflux

for 3 h followed by deprotection and chromatography on a silica gel column (CHCl_3 –MeOH, 95:5) gave **5** as a white solid (68% yield). ^1H NMR (DMSO- d_6): δ 1.52 (t, J = 7.2 Hz, 3H), 4.59 (pq, J = 4.7 Hz, 1H), 4.71 (q, J = 7.2 Hz, 4H), 4.82 (q, J = 4.9 Hz, 1H), 5.20 (d, J = 4.7 Hz, 1H), 5.75 (d, J = 5.5 Hz, 1H), 5.85 (d, J = 5.9 Hz, 1H), 6.12 (d, J = 5.1 Hz, 1H), 6.21 (d, J = 3.0 Hz, 1H), 6.37 (d, J = 2.3 Hz, 1H), 7.51 (t, J = 0.85 Hz, 1H), 8.20 (s, 1H), 8.32 (brs, 1H), 8.41 (s, 1H). ^{13}C NMR (DMSO- d_6): 14.33, 39.53, 48.51, 73.56, 73.74, 76.59, 88.32, 107.25, 112.23, 119.44, 139.83, 141.15, 143.05, 149.83, 152.45, 155.37, 164.26 ppm. MS (API-ESI): m/z 414.16 $[\text{M} + \text{H}]^+$. Anal. Calcd for $\text{C}_{17}\text{H}_{19}\text{N}_9\text{O}_4$: C, 49.39; H, 4.63; N, 30.49. Found: C, 49.38; H, 4.62; N, 30.48.

(2R,3R,4S,5R)-2-(2-Chloro-6-((furan-2-ylmethyl)amino)-9H-purin-9-yl)-5-(2-ethyl-2H-tetrazol-5-yl)tetrahydrofuran-3,4-diol (6)—Reaction of **19** with

furfurylamine at reflux for 4 h followed by deprotection and chromatography on a silica gel column (CHCl_3 –MeOH, 98:2) gave **6** as a white solid (51% yield). ^1H NMR (DMSO- d_6): δ 1.52 (t, J = 7.2 Hz, 3H), 4.55 (pq, J = 4.2 Hz, 1H), 4.62 (brs, 2H), 4.70 (q, J = 7.2 Hz, 2H), 4.78 (q, J = 5.5 Hz, 1H), 5.21 (d, J = 4.2 Hz, 1H), 5.81 (d, J = 5.5 Hz, 1H), 5.85 (d, J = 5.9 Hz, 1H), 6.05 (d, J = 5.1 Hz, 1H), 6.25 (s, 1H), 6.35 (d, 1H), 7.58 (s, 1H), 8.45 (s, 1H), 8.85 (brs, 1H). ^{13}C NMR (DMSO- d_6): 14.31, 39.26, 48.59, 73.67, 73.83, 76.22, 88.79, 107.02, 113.01, 118.89, 140.07, 141.43, 143.12, 149.56, 153.07, 155.87, 164.35 ppm. MS (API-ESI): m/z 448.12 $[\text{M} + \text{H}]^+$. Anal. Calcd for $\text{C}_{17}\text{H}_{18}\text{ClN}_9\text{O}_4$: C, 49.39; H, 4.63; N, 30.49. Found: C, 49.38; H, 4.62; N, 30.48.

(2R,3S,4R,5R)-2-(2-Ethyl-2H-tetrazol-5-yl)-5-(6-((thiophen-2-ylmethyl)amino)-9H-purin-9-yl)tetrahydrofuran-3,4-diol (7)—Reaction of **18** with 2-thiophenemethylamine at reflux for 14 h followed by deprotection and chromatography on a silica gel column (CHCl₃–MeOH, 95:5) gave **7** as a white solid (50% yield). ¹H NMR (DMSO-*d*₆): δ 1.52 (t, *J* = 7.2 Hz, 3H), 4.59 (pq, *J* = 5.1 Hz, 1H), 4.71 (q, *J* = 7.0 Hz, 2H), 4.77–4.86 (m, 3H), 5.19 (d, *J* = 4.2 Hz, 1H), 5.75 (d, *J* = 5.5 Hz, 1H), 5.85 (d, *J* = 5.9 Hz, 1H), 6.11 (d, *J* = 4.7 Hz, 1H), 6.90 (t, *J* = 4.2 Hz, 1H), 7.02 (d, *J* = 3.1 Hz, 1H), 7.30 (d, *J* = 4.7, 1H), 8.20 (s, 1H), 8.40 (s, 1H), 8.47 (brs, 1H). ¹³C NMR (DMSO-*d*₆): 14.24, 49.07, 51.73, 73.35, 73.97, 76.57, 89.03, 119.41, 125.54, 126.71, 127.35, 140.31, 141.03, 149.53, 153.31, 155.67, 164.31 ppm. MS (API-ESI): *m/z* 430.13 [M + H]⁺. Anal. Calcd for C₁₇H₁₉N₉O₃S: C, 47.55; H, 4.46; N, 29.35. Found: C, 47.56; H, 4.47; N, 29.36.

(2R,3R,4S,5R)-2-(2-Chloro-6-((thiophen-2-ylmethyl)amino)-9H-purin-9-yl)-5-(2-ethyl-2H-tetrazol-5-yl)tetrahydrofuran-3,4-diol (8)—Reaction of **19** with 2-thiophenemethylamine at reflux for 4 h followed by deprotection and chromatography on a silica gel column (CHCl₃–MeOH, 98:2) gave **8** as a white solid (76% yield). ¹H NMR (DMSO-*d*₆): δ 1.50 (t, *J* = 7.2 Hz, 3H), 4.55 (pq, *J* = 4.2 Hz, 1H), 4.71 (q, *J* = 7.4 Hz, 2H), 4.74–4.80 (m, 3H), 5.22 (d, *J* = 3.8 Hz, 1H), 5.82 (d, *J* = 5.1 Hz, 1H), 5.86 (d, *J* = 5.9 Hz, 1H), 6.05 (d, *J* = 5.1 Hz, 1H), 6.95 (t, *J* = 4.2 Hz, 1H), 7.03 (d, *J* = 3.4 Hz, 1H), 7.35 (d, *J* = 5.9, 1H), 8.41 (s, 1H), 9.03 (brs, 1H). ¹³C NMR (DMSO-*d*₆): 14.21, 48.97, 51.67, 73.22, 73.56, 76.89, 89.21, 118.57, 125.33, 126.62, 127.22, 140.56, 141.13, 149.37, 153.45, 155.58, 164.13 ppm. MS (API-ESI): *m/z* 464.09 [M + H]⁺. Anal. Calcd for C₁₇H₁₈ClN₉O₃S: C, 44.02; H, 3.91; N, 27.17. Found: C, 44.03; H, 3.92; N, 27.16.

(2R,3R,4S,5R)-2-(2-Ethyl-2H-tetrazol-5-yl)-5-(6-((3-fluorobenzyl)amino)-9H-purin-9-yl)tetrahydrofuran-3,4-diol (9)—Reaction of **18** with 3-fluorobenzylamine at reflux for 4 h followed by deprotection and chromatography on a silica gel column (CHCl₃–MeOH, 97:3) gave **9** as a white solid (72% yield). ¹H NMR (DMSO-*d*₆): δ 1.50 (t, *J* = 7.3 Hz, 3H), 4.58–4.64 (m, 1H), 4.71 (q, *J* = 7.2 Hz, 4H), 4.82 (q, *J* = 4.7 Hz, 1H), 5.18 (d, *J* = 4.3 Hz, 1H), 5.75 (d, *J* = 5.9 Hz, 1H), 5.82 (d, *J* = 5.9 Hz, 1H), 6.13 (d, *J* = 5.1 Hz, 1H), 7.02 (dt, *J* = 2.5, 8.5 Hz, 1H), 7.15 (dd, *J* = 9.2, 15.6 Hz, 2H), 7.31 (q, *J* = 7.9 Hz, 1H), 8.21 (s, 1H), 8.42 (s, 1H), 8.51 (brs, 1H). ¹³C NMR (DMSO-*d*₆): 14.61, 43.34, 48.91, 74.24, 74.51, 77.85, 88.55, 114.23, 114.35, 114.73, 118.92, 123.93, 131.11, 140.45, 143.24, 150.26, 152.22, 155.33, 164.67 ppm. MS (API-ESI): *m/z* 442.18 [M + H]⁺. Anal. Calcd for C₁₉H₂₀FN₉O₃: C, 51.70; H, 4.57; N, 28.56. Found: C, 51.71; H, 4.56; N, 28.57.

(2R,3R,4S,5R)-2-(2-Chloro-6-((3-fluorobenzyl)amino)-9H-purin-9-yl)-5-(2-ethyl-2H-tetrazol-5-yl)tetrahydrofuran-3,4-diol (10)—Reaction of **19** with 3-fluorobenzylamine at reflux for 4 h followed by deprotection and chromatography on a silica gel column (CHCl₃–MeOH, 97:3) gave **10** as a white solid (84% yield). ¹H NMR (DMSO-*d*₆): δ 1.50 (t, *J* = 7.2 Hz, 3H), 4.55 (q, *J* = 4.3 Hz, 1H), 4.64 (t, *J* = 4.9 Hz, 2H), 4.70 (q, *J* = 7.2 Hz, 2H), 4.78 (q, *J* = 5.2 Hz, 1H), 5.21 (d, *J* = 4.2 Hz, 1H), 5.81 (d, *J* = 5.5 Hz, 1H), 5.85 (d, *J* = 6.3 Hz, 1H), 6.05 (d, *J* = 5.1 Hz, 1H), 7.05 (dt, *J* = 2.1, 8.9 Hz, 1H), 7.15 (pt, *J* = 9.1 Hz, 2H), 7.34 (q, *J* = 7.9 Hz, 1H), 8.42 (s, 1H), 8.92 (brs, 1H). ¹³C NMR (DMSO-*d*₆): 14.81, 43.39, 48.94, 74.21, 74.49, 77.92, 88.46, 114.27, 114.51, 114.75, 118.87, 123.93, 131.06,

140.41, 143.21, 150.12, 153.16, 155.59, 164.78 ppm. MS (API-ESI): m/z 476.13 [M + H]⁺. Anal. Calcd for C₁₉H₁₉ClFN₉O₃: C, 47.96; H, 4.02; N, 26.49. Found: C, 47.97; H, 4.03; N, 26.47.

(2R,3S,4R,5R)-2-(6-((3-Chlorobenzyl)amino)-9H-purin-9-yl)-5-(2-ethyl-2H-tetrazol-5-yl)tetrahydrofuran-3,4-diol (11)—Reaction of **18** with 3-chlorobenzylamine at reflux for 4 h followed by deprotection and chromatography on a silica gel column (CHCl₃–MeOH, 97:3) gave **11** as a white solid (94% yield). ¹H NMR (DMSO-*d*₆): δ 1.50 (t, *J* = 7.5 Hz, 3H), 4.58–4.65 (m, 1H), 4.68 (q, *J* = 7.3 Hz, 4H), 4.83 (q, *J* = 5.1 Hz, 1H), 5.21 (d, *J* = 4.2 Hz, 1H), 5.75 (d, *J* = 5.5 Hz, 1H), 5.82 (d, *J* = 5.5 Hz, 1H), 6.10 (d, *J* = 5.1 Hz, 1H), 7.24–7.38 (m, 3H), 7.45 (brs, 1H), 8.18 (s, 1H), 8.42 (s, 1H), 8.51 (brs, 1H). ¹³C NMR (DMSO-*d*₆): 14.42, 42.94, 48.53, 73.95, 74.16, 77.33, 88.16, 118.79, 126.16, 126.93, 127.26, 130.47, 133.24, 139.46, 143.08, 148.62, 153.04, 154.73, 164.53 ppm. MS (API-ESI): m/z 458.14 [M + H]⁺. Anal. Calcd for C₁₉H₂₀ClN₉O₃: C, 49.84; H, 4.40; N, 27.53. Found: C, 49.85; H, 4.41; N, 27.54.

(2R,3R,4S,5R)-2-(2-Chloro-6-((3-chlorobenzyl)amino)-9H-purin-9-yl)-5-(2-ethyl-2H-tetrazol-5-yl)tetrahydrofuran-3,4-diol (12)—Reaction of **19** with 3-chlorobenzylamine at reflux for 4 h followed by deprotection and chromatography on a silica gel column (CHCl₃–MeOH, 98:2) gave **12** as a white solid (57% yield). ¹H NMR (DMSO-*d*₆): δ 1.50 (t, *J* = 7.2 Hz, 3H), 4.56 (q, *J* = 4.7 Hz, 1H), 4.59–4.63 (m, 2H), 4.71 (q, *J* = 7.2 Hz, 2H), 4.78 (q, *J* = 5.3 Hz, 1H), 5.21 (d, *J* = 4.2 Hz, 1H), 5.82 (d, *J* = 5.9 Hz, 1H), 5.85 (d, *J* = 5.9 Hz, 1H), 6.05 (d, *J* = 5.1 Hz, 1H), 7.24–7.43 (m, 4H), 8.43 (s, 1H), 8.91 (brs, 1H). ¹³C NMR (DMSO-*d*₆): 14.39, 43.01, 48.59, 73.91, 74.15, 77.64, 88.15, 118.88, 126.32, 127.21, 127.49, 130.58, 133.31, 140.01, 142.11, 150.32, 153.64, 155.23, 164.45 ppm. MS (API-ESI): m/z 492.10 [M + H]⁺. Anal. Calcd for C₁₉H₁₉Cl₂N₉O₃: C, 46.35; H, 3.89; N, 25.61. Found: C, 46.36; H, 3.88; N, 25.62.

(2R,3S,4R,5R)-2-(6-((3-Bromobenzyl)amino)-9H-purin-9-yl)-5-(2-ethyl-2H-tetrazol-5-yl)tetrahydrofuran-3,4-diol (13)—Reaction of **18** with 3-bromobenzylamine at reflux for 5 h followed by deprotection and chromatography on a silica gel column (CHCl₃–MeOH, 95:5) gave **13** as a white solid (58% yield). ¹H NMR (DMSO-*d*₆): δ 1.50 (t, *J* = 7.3 Hz, 3H), 4.63 (pq, *J* = 4.7 Hz, 1H), 4.69 (q, *J* = 7.3 Hz, 4H), 4.81 (q, *J* = 5.6 Hz, 1H), 5.18 (d, *J* = 4.3 Hz, 1H), 5.75 (d, *J* = 5.5 Hz, 1H), 5.82 (d, *J* = 5.9 Hz, 1H), 6.12 (d, *J* = 4.7 Hz, 1H), 7.23 (t, *J* = 7.7 Hz, 1H), 7.32 (d, *J* = 7.7 Hz, 1H), 7.38 (d, *J* = 7.7 Hz, 1H), 7.52 (brs, 1H), 8.21 (s, 1H), 8.42 (s, 1H), 8.51 (brs, 1H). ¹³C NMR (DMSO-*d*₆): 14.81, 43.05, 48.91, 74.23, 74.47, 77.61, 88.44, 119.02, 122.23, 126.86, 130.19, 130.43, 131.17, 139.86, 143.88, 150.43, 153.41, 155.23, 164.83 ppm. MS (API-ESI): m/z 502.09 [M + H]⁺. Anal. Calcd for C₁₉H₂₀BrN₉O₃: C, 45.43; H, 4.01; N, 25.10. Found: C, 45.44; H, 4.02; N, 25.11.

(2R,3R,4S,5R)-2-(6-((3-Bromobenzyl)amino)-2-chloro-9H-purin-9-yl)-5-(2-ethyl-2H-tetrazol-5-yl)tetrahydrofuran-3,4-diol (14)—Reaction of **19** with 3-bromobenzylamine at reflux for 4 h followed by deprotection and chromatography on a silica gel column (CHCl₃–MeOH, 95:5) gave **14** as a white solid (68% yield). ¹H NMR (DMSO-*d*₆): δ 1.51 (t, *J* = 7.2 Hz, 3H), 4.55 (q, *J* = 4.7 Hz, 1H), 4.63 (t, *J* = 4.7 Hz, 2H),

4.71 (q, $J = 7.2$ Hz, 2H), 4.78 (q, $J = 5.1$ Hz, 1H), 5.21 (d, $J = 4.2$ Hz, 1H), 5.82 (d, $J = 5.5$ Hz, 1H), 5.85 (d, $J = 5.9$ Hz, 1H), 6.05 (d, $J = 5.1$ Hz, 1H), 7.28 (t, $J = 7.7$, 1H), 7.32 (d, $J = 7.7$, 1H), 7.42 (d, $J = 7.7$ Hz, 1H), 7.55 (brs, 1H), 8.45 (s, 1H), 8.75 (brs, 1H). ^{13}C NMR (DMSO- d_6): 14.78, 43.31, 48.93, 74.22, 74.48, 77.61, 88.47, 119.14, 122.27, 127.06, 130.44, 130.75, 131.26, 140.42, 142.69, 150.61, 153.97, 155.51, 164.79 ppm. MS (API-ESI): m/z 536.05 $[\text{M} + \text{H}]^+$. Anal. Calcd for $\text{C}_{19}\text{H}_{19}\text{BrClN}_9\text{O}_3$: C, 42.51; H, 3.57; N, 23.49. Found: C, 42.52; H, 3.56; N, 23.48.

(2R,3R,4S,5R)-2-(2-Ethyl-2H-tetrazol-5-yl)-5-(6-((3-iodobenzyl)amino)-9H-purin-9-yl)tetrahydrofuran-3,4-diol (15)—

Reaction of **18** with 3-iodobenzylamine hydrochloride (1.1 mmol) and TEA (3.1 mmol) for 9 h followed by deprotection gave **15**, which was purified by chromatography on a silica gel column (CHCl_3 –MeOH, 98:2) as a white solid (48% yield). ^1H NMR (DMSO- d_6): δ 1.52 (t, $J = 7.3$ Hz, 3H), 4.61 (pq, $J = 4.5$ Hz, 1H), 4.64–4.68 (m, 2H), 4.72 (q, $J = 7.3$ Hz, 2H), 4.81 (q, $J = 5.2$ Hz, 1H), 5.19 (d, $J = 4.7$ Hz, 1H), 5.75 (d, $J = 5.1$ Hz, 1H), 5.82 (d, $J = 5.5$ Hz, 1H), 6.11 (d, $J = 4.7$ Hz, 1H), 7.09 (t, $J = 7.9$ Hz, 1H), 7.33 (d, $J = 7.8$ Hz, 1H), 7.55 (d, $J = 7.3$ Hz, 1H), 7.70 (brs, 1H), 8.20 (s, 1H), 8.40 (s, 1H), 8.50 (brs, 1H). ^{13}C NMR (DMSO- d_6): 14.31, 42.21, 48.73, 73.42, 74.48, 77.11, 88.08, 93.96, 118.87, 126.37, 130.06, 135.11, 135.74, 140.58, 143.01, 149.22, 153.02, 154.65, 164.39 ppm. MS (API-ESI): m/z 550.07 $[\text{M} + \text{H}]^+$. Anal. Calcd for $\text{C}_{19}\text{H}_{20}\text{IN}_9\text{O}_3$: C, 41.54; H, 3.67; N, 22.95. Found: C, 41.55; H, 3.66; N, 22.96.

(2R,3S,4R,5R)-2-(6-((4-Chloro-2-fluorobenzyl)amino)-9H-purin-9-yl)-5-(2-ethyl-2H-tetrazol-5-yl)tetrahydrofuran-3,4-diol (16)—

Reaction of **18** with 4-chloro-2-fluorobenzylamine hydrochloride (1.1 mmol) and TEA (3.1 mmol) for 8 h followed by deprotection gave **16**, which was purified by chromatography on a silica gel column (CHCl_3 –MeOH, 95:5) as a white solid (76% yield). ^1H NMR (DMSO- d_6): δ 1.50 (t, $J = 7.3$ Hz, 3H), 4.62 (pq, $J = 4.7$ Hz, 1H), 4.73 (q, $J = 7.4$ Hz, 4H), 4.81 (pq, $J = 4.7$ Hz, 1H), 5.21 (d, $J = 4.7$ Hz, 1H), 5.78 (d, $J = 5.5$ Hz, 1H), 5.82 (d, $J = 5.9$ Hz, 1H), 6.13 (d, $J = 4.7$ Hz, 1H), 7.19 (dd, $J = 1.7, 8.5$ Hz, 1H), 7.31 (t, $J = 8.1$ Hz, 1H), 7.39 (dd, $J = 1.9, 10.1$ Hz, 1H), 8.20 (s, 1H), 8.45 (s, 1H), 8.47 (brs, 1H). ^{13}C NMR (DMSO- d_6): 14.43, 38.21, 48.56, 73.93, 74.15, 77.35, 88.15, 115.74, 116.24, 119.24, 124.81, 124.87, 130.68, 133.21, 139.56, 149.76, 153.02, 155.03, 164.52 ppm. MS (API-ESI): m/z 476.13 $[\text{M} + \text{H}]^+$. Anal. Calcd for $\text{C}_{19}\text{H}_{19}\text{ClFN}_9\text{O}_3$: C, 47.96; H, 4.02; N, 22.49. Found: C, 47.95; H, 4.03; N, 22.47.

(2R,3R,4S,5R)-2-(2-Chloro-6-((4-chloro-2-fluorobenzyl)-amino)-9H-purin-9-yl)-5-(2-ethyl-2H-tetrazol-5-yl)-tetrahydrofuran-3,4-diol (17)—

Reaction of **19** with 4-chloro-2-fluorobenzylamine hydrochloride (1.1 mmol) and TEA (3.1 mmol) for 8 h followed by deprotection gave **17**, which was purified by chromatography on a silica gel column (CHCl_3 –MeOH, 95:5) as a white solid (52% yield). ^1H NMR (DMSO- d_6): δ 1.52 (t, $J = 7.2$ Hz, 3H), 4.53 (pq, $J = 4.6$ Hz, 1H), 4.61–4.66 (m, 2H), 4.71 (q, $J = 7.3$ Hz, 2H), 4.78 (pq, $J = 4.7$ Hz, 1H), 5.21 (d, $J = 3.8$ Hz, 1H), 5.81 (d, $J = 5.5$ Hz, 1H), 5.85 (d, $J = 5.9$ Hz, 1H), 6.05 (d, $J = 5.1$ Hz, 1H), 7.20 (d, $J = 7.6$ Hz, 1H), 7.32 (t, $J = 7.9$ Hz, 1H), 7.40 (dd, $J = 1.9, 10.1$ Hz, 1H), 8.43 (s, 1H), 8.92 (brs, 1H). ^{13}C NMR (DMSO- d_6): 14.76, 39.45, 48.93, 74.16, 74.45, 77.92, 88.41, 116.33, 116.58, 119.18, 125.27, 131.27, 131.32, 133.03, 140.48,

150.63, 153.92, 155.51, 164.76 ppm. MS (API-ESI): m/z 510.09 [M + H]⁺. Anal. Calcd for C₁₉H₁₈Cl₂FN₉O₃: C, 44.72; H, 3.56; N, 24.70. Found: C, 44.73; H, 3.57; N, 24.71.

Membrane Preparation

Membranes for radioligand binding were prepared as described earlier.¹⁹ In brief, after homogenization of CHO cells stably transfected with the human AR subtypes or rat A₃ AR membranes were prepared in a two-step procedure. A first low-speed centrifugation (1000*g*) was used to remove cell fragments and nuclei and was followed by a high-speed centrifugation (100 000*g*) of the supernatant in order to sediment a crude membrane fraction. The resulting membrane pellets were resuspended in the buffer used for the respective binding experiments, frozen in liquid nitrogen, and stored in aliquots at -80 °C. Adenylyl cyclase activity was measured in a membrane fraction obtained in a simplified procedure with only one high-speed centrifugation of the homogenate. The resulting crude membrane pellet was resuspended in 50 mM Tris/HCl, pH 7.4, and used immediately for the cyclase assay.

Radioligand Binding and Adenylyl Cyclase Assay

In competition experiments the following radioligands were used: 1 nM [³H]CCPA for hA₁ receptors, 10 nM [³H]NECA for hA_{2A} ARs, 1 nM [³H]HEMADO for hA₃ ARs, and 30 nM [³H]NECA for rA₃ ARs.^{19,40} Nonspecific binding of [³H]CCPA was determined in the presence of 1 mM theophylline, while nonspecific binding of [³H]NECA and [³H]HEMADO was estimated in the presence of 100 μM R-PIA. Dissociation constants (K_i values) were calculated from radioligand competition experiments utilizing the program Prism (GraphPad).

Due to the lack of a useful high-affinity radioligand for A_{2B} ARs, stimulation of adenylyl cyclase activity was measured to determine agonist potency (EC₅₀ values).¹⁹ If only partial agonistic activity was observed, efficacy was compared to 100 μM NECA⁴¹ as a full agonist. All values are given as geometric means with 95% confidence intervals ($n = 3$). The functional activity at the hA₁, A_{2A}, and A₃ receptors was determined in adenylyl cyclase experiments. The inhibition of forskolin-stimulated adenylyl cyclase via hA₁ and A₃ receptors was measured as described earlier.^{19,42} As reference agonists (efficacy = 100%), CCPA⁴³ and NECA, respectively, were used. Compounds were considered to be A₃ antagonists if they fully reversed (>85%) the NECA-mediated inhibition of adenylyl cyclase activity (EC₅₀ values in Table 2). The functional activity of selected derivatives at the rat A₃ receptor was also determined in adenylyl cyclase experiments. Functional A_{2A} activity was determined as described for A_{2B} adenosine receptors (see above and ref 19).

Formalin Test

The experimental procedures applied in the formalin test were approved by the Animal Ethics Committee of the University of Campania. Animal care was in compliance with the IASP and European Community guidelines on the use and protection of animals in experimental research (E.C. L358/118/12/86). All efforts were made to minimize animal suffering and to reduce the number of animals used. Formalin injection induces a biphasic stereotypical nocifensive behavior.³⁷ Nociceptive responses are divided into an early, short

lasting first phase (0–7 min) caused by a primary afferent discharge produced by the stimulus, followed by a quiescent period and then a second, prolonged phase (15–60 min) of tonic pain. Mice received formalin (1.25% in saline, 30 μL) in the dorsal surface of one side of the hind paw. Each mouse was randomly assigned to one of the experimental groups ($n = 8–10$) and placed in a Plexiglas cage and allowed to move freely for 15–20 min. A mirror was placed at a 45° angle under the cage to allow full view of the hind paws. Lifting, favoring, licking, shaking, and flinching of the injected paw were recorded as nociceptive responses. The total time of the nociceptive response was measured every 5 min and expressed as the total time of the nociceptive responses in minutes (mean \pm SEM). Recording of nociceptive behavior commenced immediately after formalin injection and was continued for 60 min. The version of the formalin test we applied is based on the fact that a correlational analysis showed that no single behavioral measure can be a strong predictor of formalin or drug concentrations on spontaneous behaviors.⁴⁴ Consistently, we considered that a simple sum of time spent licking plus elevating the paw, or the weighted pain score, is in fact superior to any single (lifting, favoring, licking, shaking and, flinching) measure (r ranging from 0.75 to 0.86).⁴⁵ For treatments, groups of 8–10 animals per treatment were used with each animal being used for one treatment only. Mice received intraperitoneal vehicle (10% DMSO in 0.9% NaCl) or different doses of **11**, **22**, **26**, **28**, **30**, and **31**. **30** was purchased from Tocris. **28** and **31** were synthesized in our laboratory as previously reported.^{16,46}

Computational Chemistry

Molecular modeling and graphics manipulations were performed using MOE (Molecular Operating Environment, version 2013.08, Chemical Computing Group, Toronto, Canada) and UCSF-CHIMERA 1.8.1 (<http://www.cgl.ucsf.edu/chimera>) software packages, running on an E4 Computer Engineering E1080 workstation provided with an Intel Xeon processor. GOLD Suite 5.4.1 docking package (CCDC Software Limited: Cambridge, U.K., 2008)²⁵ was used for all docking calculations. Figures were generated using Pymol 1.8.2 (Schrödinger, LLC, New York, NY, 2016).

Residue Indexing

The Ballesteros–Weinstein double-numbering system²⁸ was used to describe the transmembrane (TM) location of the amino acids. Along with numbering their positions in the primary amino acid sequence, the residues have numbers in parentheses ($X.YZ$) that indicate their position in each transmembrane (TM) helix (X), relative to a conserved reference residue in that TM helix (YZ).

3D Structures of hA₁AR and hA₃AR

As, to date, no crystallographic information about the hA₁AR and hA₃AR is available, previously reported molecular models,^{20,47} built using the alignment and the homology modeling tools implemented in the program MOE, were used in this study. The hA₁AR homology model was built using as template the crystal structure of the human A_{2A}AR cocrystallized with the agonist UK-432097 (PDB code 3QAK).²¹ The 3QAK structure was also selected as a template for the entire A₃AR structure except for the extracellular terminus

of TM2 (residues from V63 to S73) and EL1 (residues from L74 to Y81). The X-ray structure of the h β_2 adrenergic receptor in complex with the G_s protein (PDB code 3SN6),⁴⁸ after superimposition with the hA_{2A}AR crystal structure, was set as template for the extracellular terminus of TM2. No structural templates were used to model the EL1. Details of the modeling procedure have been previously described.^{22,47} In particular, the hA₁AR and hA₃AR sequences were retrieved from the publicly available sequence database www.uniprot.org and aligned against the sequence of the respective A_{2A}AR and hybrid A_{2A}AR- β_2 adrenergic receptor templates, taking into account the highly conserved residues in each TM domain and following the numbering scheme by Ballesteros and Weinstein.²⁸ Then, homology models were built using the automated Homology Modeling protocol implemented in the MOE suite.

Docking Simulations of 5'-C-(Ethyltetrazol-2-yl)adenosine Derivatives at the hA₁AR and hA₃AR Models

Structures of compounds **9**, **11**, **13**, and **15** were built using the builder tool implemented in the MOE suite and subjected to a MMFF94x energy minimization until a rms gradient was $<0.05 \text{ kcal mol}^{-1} \text{ \AA}^{-1}$. Molecular docking was performed by means of the GOLD software, which uses a genetic algorithm and considers full ligand conformational flexibility and partial protein flexibility, i.e., the flexibility of side chain residues only. The coordinates of four key residues in the binding pocket of both hA₁AR and hA₃AR models, that is, F (EL2), N^{6.55}, W^{6.48}, and H^{7.43}, were chosen as active-site origin. The active-site radius was set equal to 13 Å. The mobility of residues at positions 3.36, 6.48, 6.52, 7.43, 6.55, 6.66 (only for hA₁AR), and 7.42 side chains was set up using the flexible side chains option in the GOLD front end, which incorporates the Lovell rotamer library.⁴⁹ Each GA run used the default parameters of 100 000 genetic operations on an initial population of 100 members divided into five subpopulations, with weights for crossover, mutation, and migration being set to 95, 95, and 10, respectively. GOLD allows a user-definable number of GA runs per ligand, each of which starts from a different orientation. For these experiments, the number of GA runs was set to 200 without the option of early termination, and scoring of the docked poses was performed with the original ChemPLP scoring function followed by rescoring with ChemScore.²⁶ The top scoring docking conformations for each ligand were subjected to visual inspection and analysis of protein–ligand interactions to select the proposed binding conformations in agreement with the experimental data.

Supplementary Material

Refer to Web version on PubMed Central for supplementary material.

Acknowledgments

We express our gratitude to Prof. Mario Grifantini and Prof. Palmarisa Franchetti for their suggestions and comments for this manuscript. This work was supported by grants from the University of Camerino (FAR 2014/15, Fondo di Ateneo per la Ricerca, Grant FPI000044), by the Italian MIUR funds (PRIN 2009, Prot. N. 20094BJ9R7 and PRIN 2009, Prot. N. 200928EEX4_004), and by the NIDDK Intramural Research Program.

ABBREVIATIONS USED**A₁AR**A₁ adenosine receptor**A_{2A}AR**A_{2A} adenosine receptor**A_{2B}AR**A_{2B} adenosine receptor**A₃AR**A₃ adenosine receptor**cAMP**

cyclic adenosine 5'-monophosphate

CCI

chronic constriction injury

CCPA2-chloro-*N*⁶-cyclopentyladenosine**CHO**

Chinese hamster ovary

2-CI-IBMECA2-chloro-*N*⁶-(3-iodobenzyl)-5'-*N*-methylcarboxamidoadenosine**5'CI5'd-(±)-ENBA and 5'CIENBA**5'-chloro-5'-deoxy-*N*⁶-(±)-(endo-norborn-2-yl)adenosine**DPCPX**

8-cyclopentyl-1,3-dipropylxanthine

EL

extracellular loop

GPCR

G-protein-coupled receptor

HEMADO2-(hexyn-1-yl)-*N*⁶-methyladenosine**ip**

intraperitoneal

NECA5'-*N*-ethylcarboxamidoadenosine

R-PIA*(R)*-*N*⁶-phenylisopropyladenosine**TEA**

triethylamine

TM

transmembrane domain

References

- Jacobson KA, Muller CE. Medicinal chemistry of adenosine, P2Y and P2X receptors. *Neuropharmacology*. 2016; 104:31–49. [PubMed: 26686393]
- Beamer E, Goloncser F, Horvath G, Beko K, Otrókocsi L, Kovanyi B, Sperlagh B. Purinergic mechanisms in neuroinflammation: An update from molecules to behavior. *Neuropharmacology*. 2016; 104:94–10. [PubMed: 26384652]
- Lavecchia A, Cerchia C. *In silico* methods to address polypharmacology: current status, applications and future perspectives. *Drug Discovery Today*. 2016; 21:288–298. [PubMed: 26743596]
- Anighoro A, Bajorath J, Rastelli G. Polypharmacology: challenges and opportunities in drug discovery. *J Med Chem*. 2014; 57:7874–7887. [PubMed: 24946140]
- Bevan N, Butchers R, Cousins R, Coates J, Edgar V, Morrison V, Sheehan J, Reeves J, Wilson DJ. Pharmacological characterisation and inhibitory effects of (2R,3R,4S,5R)-2-(6-amino-2-[[[(1S)-2-hydroxy-1-(phenylmethyl)ethyl]amino]-9H-purin-9-yl]-5-(2-ethyl-2H-tetrazol-5-yl)tetrahydro-3,4-furandiyl, a novel ligand that demonstrates both adenosine A_{2A} receptor agonist and adenosine A₃ receptor antagonist activity. *Eur J Pharmacol*. 2007; 564:219–225. [PubMed: 17382926]
- Hou X, Majik MS, Kim K, Pyee Y, Lee Y, Alexander V, Chung HJ, Lee HW, Chandra G, Lee H, Park S, Choi WJ, Kim O, Phan K, Gao G, Jacobson KA, Choi S, Lee SK, Jeong LS. Structure–activity relationships of truncated C2- or C8-substituted adenosine derivatives as dual acting A_{2A} and A₃ adenosine receptor ligands. *J Med Chem*. 2012; 55:342–356. [PubMed: 22142423]
- Petrelli R, Torquati I, Kachler S, Luongo L, Maione S, Franchetti P, Grifantini M, Novellino E, Lavecchia A, Klotz KN, Cappellacci L. 5′-C-tetrazolyl-*N*⁶-substituted adenosine and 2-chloroadenosine derivatives as highly potent dual acting A₁ adenosine receptor agonists and A₃ adenosine receptor antagonists. *J Med Chem*. 2015; 58:2560–2566. [PubMed: 25699637]
- Borea PA, Varani K, Vincenzi F, Baraldi PG, Tabrizi MA, Merighi S, Gessi S. The A₃ adenosine receptor: history and perspectives. *Pharmacol Rev*. 2015; 67:74–102. [PubMed: 25387804]
- Chen Z, Janes K, Chen C, Doyle T, Bryant L, Tosh DK, Jacobson KA, Salvemini D. Controlling murine and rat chronic pain through A₃ adenosine receptor activation. *FASEB J*. 2012; 26:1855–1865. [PubMed: 22345405]
- Varani K, Vincenzi F, Targa T, Paradiso B, Parrilli A, Fini M, Lanza G, Borea PA. The stimulation of A₃ adenosine receptors reduces bone-residing breast cancer in a rat preclinical model. *Eur J Cancer*. 2013; 49:482–491. [PubMed: 22770890]
- Tosh DK, Finley A, Paoletta S, Moss SM, Gao ZG, Gizewski ET, Auchampach JA, Salvemini D, Jacobson KA. *In Vivo* phenotypic screening for treating chronic neuropathic pain: modification of C2-arylethynyl group of conformationally constrained A₃ adenosine receptor agonists. *J Med Chem*. 2014; 57:9901–9914. [PubMed: 25422861]
- Little JW, Ford A, Symons-Liguori AM, Chen Z, Janes K, Doyle T, Xie J, Luongo L, Tosh DK, Maione S, Bannister K, Dickenson AH, Vanderah TW, Porreca F, Jacobson KA, Salvemini D. Endogenous adenosine A₃ receptor activation selectively alleviates persistent pain states. *Brain*. 2015; 138:28–35. [PubMed: 25414036]
- Janes K, Symons-Liguori AM, Jacobson KA, Salvemini D. Identification of A₃ adenosine receptor agonists as novel non-narcotic analgesic. *Br J Pharmacol*. 2016; 173:1253–1267. [PubMed: 26804983]

14. Yan H, Zhang E, Feng C, Zhao X. Role of A₃ adenosine receptor in diabetic neuropathy. *J Neurosci Res.* 2016; 94:936–946. [PubMed: 27319979]
15. Maione S, De Novellis V, Cappellacci L, Palazzo E, Vita D, Luongo L, Stella L, Franchetti P, Marabese I, Rossi F, Grifantini M. The antinociceptive effect of 2-chloro-2'-*C*-methyl-*N*⁶-cyclopentyladenosine (2'-Me-CCPA), a highly selective adenosine A₁ receptor agonist, in the rat. *Pain.* 2007; 131:281–292. [PubMed: 17317007]
16. Franchetti P, Cappellacci L, Vita P, Petrelli R, Lavecchia A, Kachler S, Klotz KN, Marabese I, Luongo L, Maione S, Grifantini M. *N*⁶-Cycloalkyl- and *N*⁶-bicycloalkyl-C5'(C2')-modified adenosine derivatives as high-affinity and selective agonists at the human A₁ adenosine receptor with antinociceptive effects in mice. *J Med Chem.* 2009; 52:2393–2406. [PubMed: 19317449]
17. Luongo L, Petrelli R, Gatta L, Giordano C, Guida F, Vita P, Franchetti P, Grifantini M, De Novellis V, Cappellacci L, Maione S. 5'-Chloro-5'-deoxy-ENBA, a potent and selective adenosine A₁ receptor agonist, alleviates neuropathic pain in mice through functional glial and microglial changes without affecting motor and cardiovascular functions. *Molecules.* 2012; 17:13712–13726. [PubMed: 23174891]
18. Petrelli R, Grifantini M, Cappellacci L. Development of C-methyl branched purine ribonucleoside analogs: chemistry, biological activity and therapeutic potential. *Curr Med Chem.* 2016; 23:3118–3135. [PubMed: 27356543]
19. Klotz KN, Hessling J, Hegler J, Owman B, Kull B, Fredholm BB, Lohse MJ. Comparative pharmacology of human adenosine receptor subtypes-characterization of stably transfected receptors in CHO cells. *Naunyn-Schmiedeberg's Arch Pharmacol.* 1997; 357:1–9.
20. Nayak A, Chandra G, Hwang I, Kim K, Hou X, Kim HO, Sahu PK, Roy KK, Yoo J, Lee Y, Cui M, Choi S, Moss SM, Phan K, Gao ZG, Ha H, Jacobson KA, Jeong LS. Synthesis and anti-renal fibrosis activity of conformationally locked truncated 2-hexynyl-N(6)-substituted-(N)-methanocarba-nucleosides as A₃ adenosine receptor antagonists and partial agonists. *J Med Chem.* 2014; 57:1344–1354. [PubMed: 24456490]
21. Tosh DK, Phan K, Deflorian F, Wei Q, Gao Z, Jacobson KA. Truncated (*N*)-methanocarba nucleosides as A₁ adenosine receptor agonists and partial agonists: overcoming lack of a recognition element. *ACS Med Chem Lett.* 2011; 2:626–631. [PubMed: 21858244]
22. Xu F, Wu H, Katritch V, Han GW, Jacobson KA, Gao ZG, Cherezov V, Stevens R. Agonist bound structure of the human adenosine A_{2A} receptor. *Science.* 2011; 332:322–327. [PubMed: 21393508]
23. Paoletta S, Tosh DK, Finley A, Gizewski E, Moss SM, Gao ZG, Auchampach JA, Salvemini D, Jacobson KA. Rational design of sulfonated A₃ adenosine receptor-selective nucleosides as pharmacological tools to study chronic neuropathic pain. *J Med Chem.* 2013; 56:5949–5963. [PubMed: 23789857]
24. Jeong LS, Lee HW, Jacobson KA, Kim HO, Shin DH, Lee JA, Gao ZG, Lu C, Duong HT, Gunaga P, Lee SK, Jin DZ, Chun MW, Moon HR. Structure-activity relationships of 2-chloro-*N*⁶-substituted-4'-thioadenosine-5'-uronamides as highly potent and selective agonists at the human A₃ adenosine receptor. *J Med Chem.* 2006; 49:273–281. [PubMed: 16392812]
25. Jones G, Willett P, Glen RC, Leach AR, Taylor R. Development and validation of a genetic algorithm for flexible docking. *J Mol Biol.* 1997; 267:727–748. [PubMed: 9126849]
26. Verdonk ML, Giangreco I, Hall RJ, Korb O, Mortenson N, Murray W. Docking performance of fragments and druglike compounds. *J Med Chem.* 2011; 54:5422–5431. [PubMed: 21692478]
27. Verdonk ML, Cole JC, Hartshorn MJ, Murray CW, Taylor RD. Improved protein-ligand docking using GOLD. *Proteins: Struct, Funct Genet.* 2003; 52:609–623. [PubMed: 12910460]
28. Ballesteros JA, Weinstein H. Integrated methods for the construction of three dimensional models and computational probing of structure-function relationships in G-protein coupled receptors. *Methods Neurosci.* 1995; 25:366–428.
29. Lebon G, Warne T, Edwards PC, Bennett K, Langmead CJ, Leslie AGW, Tate CG. Agonist-bound adenosine A_{2A} receptor structures reveal common features of GPCR activation. *Nature.* 2011; 474:521–525. [PubMed: 21593763]

30. Kim SK, Gao ZG, Van Rompaey P, Gross AS, Chen A, Van Calenbergh S, Jacobson KA. Modeling the adenosine receptors: comparison of the binding domains of A_{2A} agonists and antagonists. *J Med Chem.* 2003; 46:4847–4859. [PubMed: 14584936]
31. Rivkees SA, Barbaiya H, IJzerman AP. Identification of the adenine binding site of the human A₁ adenosine receptor. *J Biol Chem.* 1999; 274:3617–3621. [PubMed: 9920910]
32. Kolá MH, Hobza P. Computer modeling of halogen bonds and other σ -hole interactions. *Chem Rev.* 2016; 116:5155–5187. [PubMed: 26840433]
33. Bondi A. Van der Waals volumes and radii. *J Phys Chem.* 1964; 68:441–451.
34. Cavallo G, Metrangolo P, Milani R, Pilati T, Priimagi A, Resnati G, Terraneo G. The halogen bond. *Chem Rev.* 2016; 116:2478–2601. [PubMed: 26812185]
35. Lange A, Zimmermann M, Wilcken R, Zahn S, Boeckler F. Targeting histidine side chains in molecular design through nitrogen-halogen bonds. *J Chem Inf Model.* 2013; 53:3178–3189. [PubMed: 24127844]
36. Beno BR, Yeung KS, Bartberger MD, Pennington LD, Meanwell NA. A survey of the role of noncovalent sulfur interactions in drug design. *J Med Chem.* 2015; 58:4383–4438. [PubMed: 25734370]
37. Dubuisson D, Dennis SG. The formalin test: a quantitative study of the analgesic effects of morphine, meperidine, and brain stem stimulation in rats and cats. *Pain.* 1977; 4:161–174. [PubMed: 564014]
38. Jacobson KA, Klutz AM, Tosh DK, Ivanov AA, Preti D, Baraldi PG. Medicinal chemistry of the A₃ adenosine receptor: agonists, antagonists, and receptor engineering. *Handb Exp Pharmacol.* 2009; 193:123–159.
39. Carlin JL, Jain S, Gizewski E, Wan TC, Tosh DK, Xiao C, Auchampach JA, Jacobson KA, Gavrilova O, Reitman ML. Hypothermia in mouse is caused by adenosine A₁ and A₃ receptor agonists and AMP via three distinct mechanisms. *Neuropharmacology.* 2017; 114:101–113. [PubMed: 27914963]
40. Klotz KN, Kachler S, Falgner N, Volpini R, Dal Ben D, Lambertucci C, Mishra RC, Vittori S, Cristalli G. [³H]-HEMADO-a novel highly potent and selective radiolabeled agonist for A₃ adenosine receptors. *Eur J Pharmacol.* 2007; 556:14–18. [PubMed: 17126322]
41. Prasad RN, Bariana DS, Fung A, Savic M, Tietje K, Stein HH, Brondyk HD, Egan RS. Modification of the 5'-position of purine nucleosides. 2. Synthesis and some cardiovascular properties of adenosine-5'-(N-substituted)carboxamides. *J Med Chem.* 1980; 23:313–319. [PubMed: 7365748]
42. Klotz KN, Cristalli G, Grifantini M, Vittori S, Lohse MJ. Photoaffinity labeling of A₁-adenosine receptors. *J Biol Chem.* 1985; 260:14659–14664. [PubMed: 2997218]
43. Lohse MJ, Klotz KN, Schwabe U, Cristalli G, Vittori S, Grifantini M. 2-Chloro-N⁶-cyclopentyladenosine: a highly selective agonist at A₁ adenosine receptors. *Naunyn-Schmiedeberg's Arch Pharmacol.* 1988; 337:687–689. [PubMed: 3216901]
44. Saggi G, Abbott FV. The formalin test in the mouse: a parametric analysis of scoring properties. *Pain.* 2000; 89:53–63. [PubMed: 11113293]
45. Abbott FV, Franklin KB, Westbrook RF. The formalin test: scoring properties of the first and second phases of the pain response in rats. *Pain.* 1995; 60:91–102. [PubMed: 7715946]
46. Cappellacci L, Franchetti P, Pasqualini M, Petrelli R, Vita P, Lavecchia A, Novellino E, Costa B, Martini C, Klotz KN, Grifantini M. Synthesis, biological evaluation, and molecular modeling of ribose-modified adenosine analogues as adenosine receptor agonists. *J Med Chem.* 2005; 48:1550–1562. [PubMed: 15743197]
47. Tosh DK, Deflorian F, Phan K, Gao ZG, Wan TC, Gizewski E, Auchampach JA, Jacobson KA. Structure-guided design of A₃ adenosine receptor-selective nucleosides: Combination of 2-arylethynyl and bicyclo[3.1.0]hexane substitutions. *J Med Chem.* 2012; 55:4847–4860. [PubMed: 22559880]
48. Rasmussen SGF, DeVree BT, Zou Y, Kruse AC, Chung KY, Kobilka TS, Thian FS, Chae PS, Pardon E, Calinski D, Mathiesen JM, Shah STA, Lyons JA, Caffrey M, Gellman SH, Steyaert J, Skinotis G, Weis WI, Sunahara RK, Kobilka BK. Crystal structure of the β_2 adrenergic receptor-Gs protein complex. *Nature.* 2011; 477:549–555. [PubMed: 21772288]

49. Lovell SC, Word JM, Richardson JS, Richardson DC. The penultimate rotamer library. *Proteins: Struct, Funct Genet.* 2000; 40:389–408. [PubMed: 10861930]

Author Manuscript

Author Manuscript

Author Manuscript

Author Manuscript

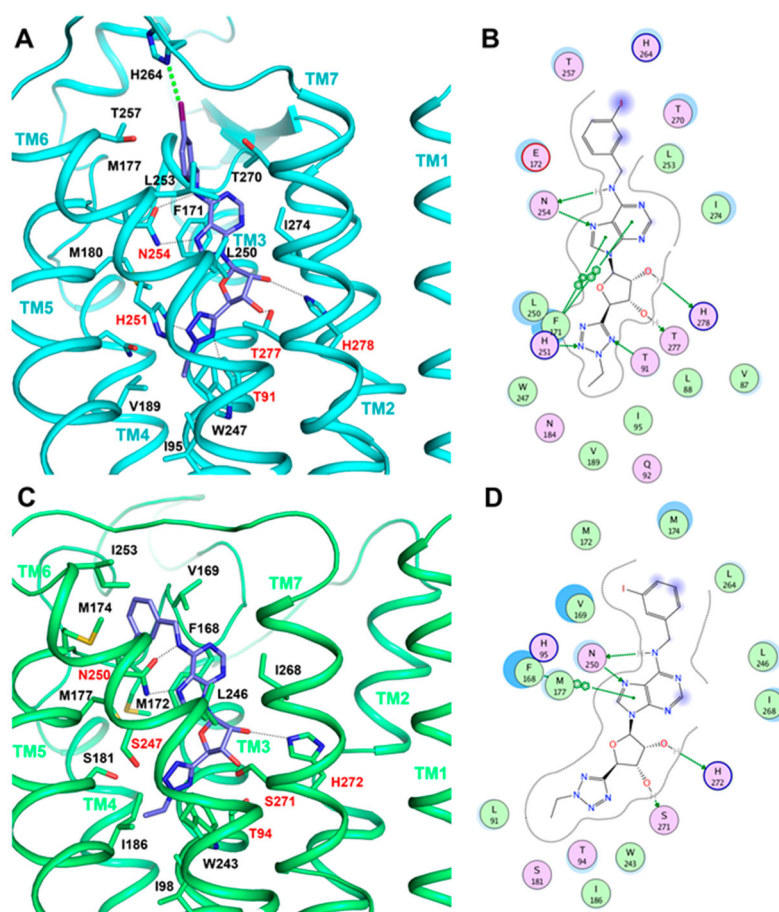


Figure 1. Putative binding mode of 5'-C-(ethyltetrazol-2-yl)adenosine derivative **15** (purple carbons) obtained after docking simulations at the hA₁AR (A, cyan ribbons) and hA₃AR (C, green ribbons) models. Poses are viewed from the membrane side. Ligands and interacting key residues are represented as stick models. The amino acids important for ligand recognition are labeled in red. H-bonding interactions are pictured as dotted black lines, and nonpolar hydrogens are undisplayed for clarity. The halogen bond of **15** to His264^{6,66} in hA₁AR is highlighted as a green dashed line. 2D diagram of interactions between **15** and both hA₁AR (B) and hA₃AR (D) models generated by the MOE software package (MOE 2013.08, Chemical Computing Group, Inc.): green spheres = “greasy” residues; spheres with red outline = acidic residues; spheres with blue outline = basic residues; spheres with black outline = polar residues; blue background spheres = receptor exposure to solvent; blue spheres on ligand atoms = ligand exposure to solvent; green dotted lines = side chain donors/acceptors; gray dotted line = proximity contour. A naphthyl icon represents a π - π stacking interaction.

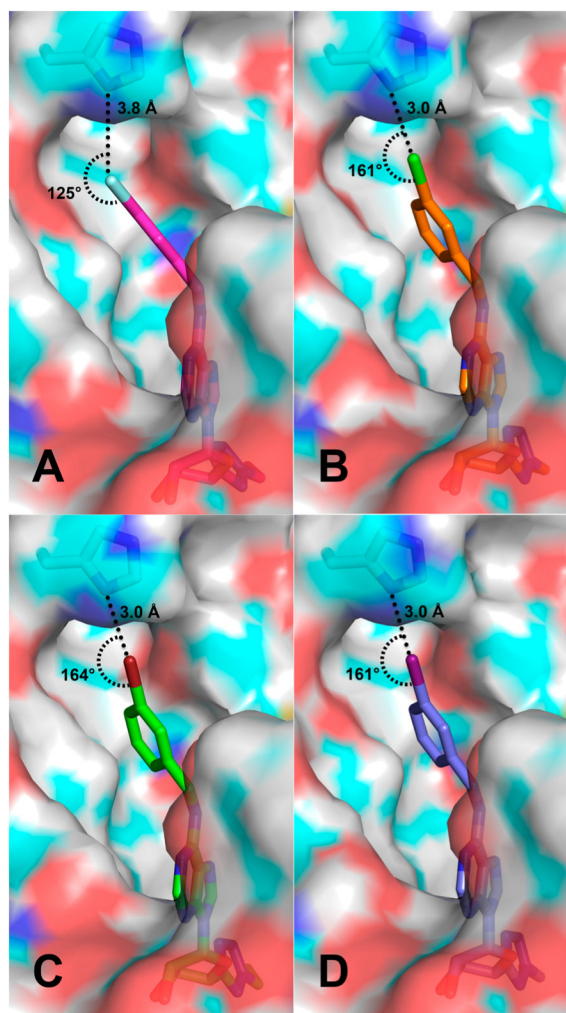


Figure 2. Close-up of the interaction between the N^{δ} atom of H264^{6.66} in the hA₁AR hydrophobic pocket and the 3-F-benzyl derivative **9** (A, magenta carbons), 3-Cl-benzyl derivative **11** (B, orange carbons), 3-Br-benzyl derivative **13** (C, green carbons), and 3-I-benzyl derivative **15** (D, purple carbons).

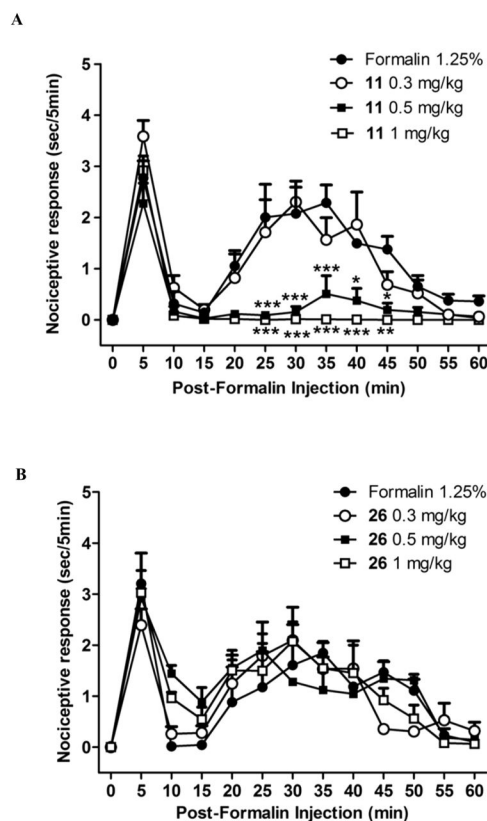


Figure 3. Effect of subcutaneous formalin (1.25%, 30 μ L) injections into the hind paw of mice on the time course of the nociceptive behaviors. Formalin was injected 10 min after the systemic administration of vehicle (0.9% NaCl, ip) or drugs. Part A shows the effects of the systemic administration of **11** (0.3, 0.5, 1 mg/kg, ip). Part B shows the effects of the systemic administration of **26** (0.3, 0.5, and 1 mg/kg, ip). Recording of nocifensive behavior began immediately after the injection of formalin (time 0) and was continued for 60 min. Each point represents the total time of the nociceptive responses (mean (SEM) of 8 mice per group, measured every 5 min. * indicates significant differences versus vehicle. $P < 0.05$ was considered statistically significant.

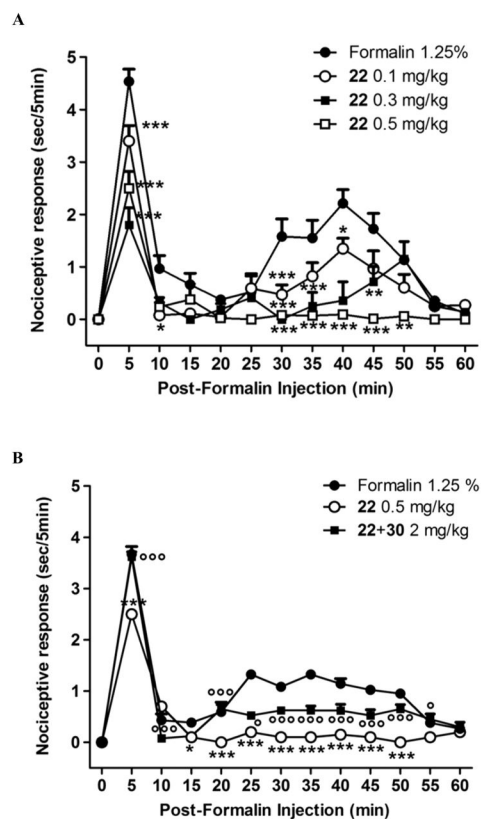


Figure 4.

Effect of subcutaneous formalin (1.25%, 30 μ L) injections into the hind paw of mice on the time course of the nociceptive behaviors. Formalin was injected 10 min after the systemic administration of vehicle (0.9% NaCl, ip) or drugs. Part A shows the effects of the systemic administration of **22** (0.1, 0.3, and 0.5 mg/kg, ip). Part B shows the effects of the systemic administration of **22** (0.5 mg/kg, ip) in combination with **30** (2 mg/kg, ip) an A_3AR antagonist. Recording of nocifensive behavior began immediately after the injection of formalin (time 0) and was continued for 60 min. Each point represents the total time of the nociceptive responses (mean (SEM) of 8 mice per group, measured every 5 min). * indicates significant differences versus vehicle and ○ indicates significant differences versus **22** 0.5 mg/kg. $P < 0.05$ was considered statistically significant.

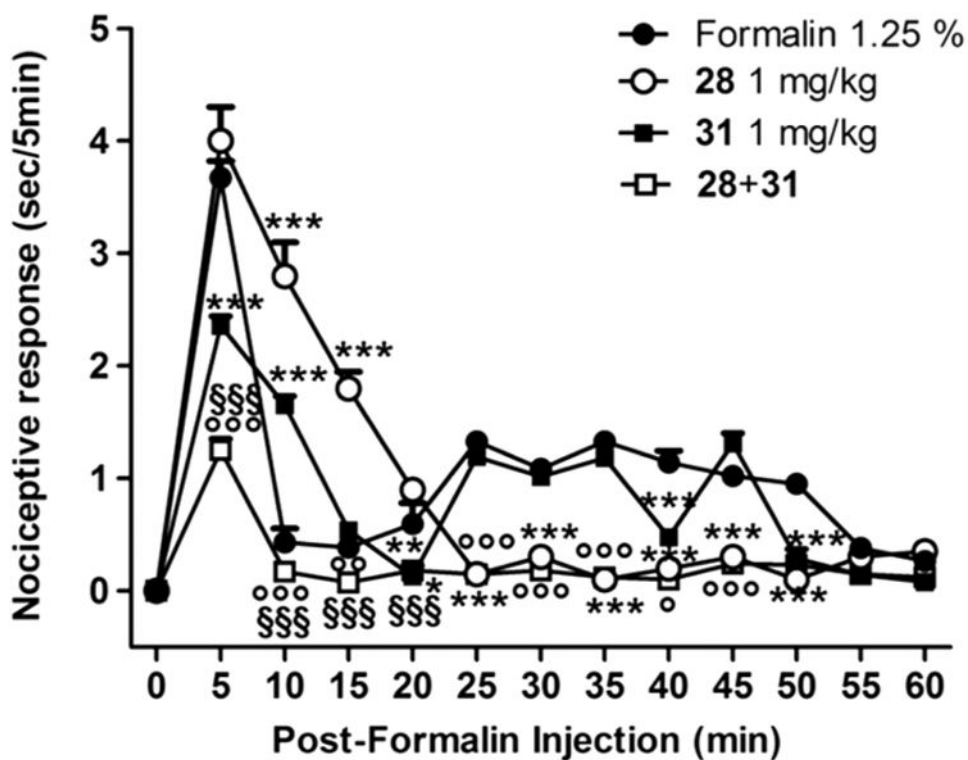


Figure 5. Effect of subcutaneous formalin (1.25%, 30 μ L) injections into the hind paw of mice on the time course of the nociceptive behaviors. Formalin was injected 10 min after the systemic administration of vehicle (0.9% NaCl, ip) or drugs. Effects of the systemic administration of **28** (1 mg/kg, ip) and **31** (1 mg/kg, ip) alone or in combination. Recording of nocifensive behavior began immediately after the injection of formalin (time 0) and was continued for 60 min. Each point represents the total time of the nociceptive responses (mean (SEM) of 8 mice per group, measured every 5 min. * indicates significant differences versus vehicle, O indicates significant differences versus **28** (1 mg/kg), and § indicates significant differences versus **31** (1 mg/kg). $P < 0.05$ was considered statistically significant.

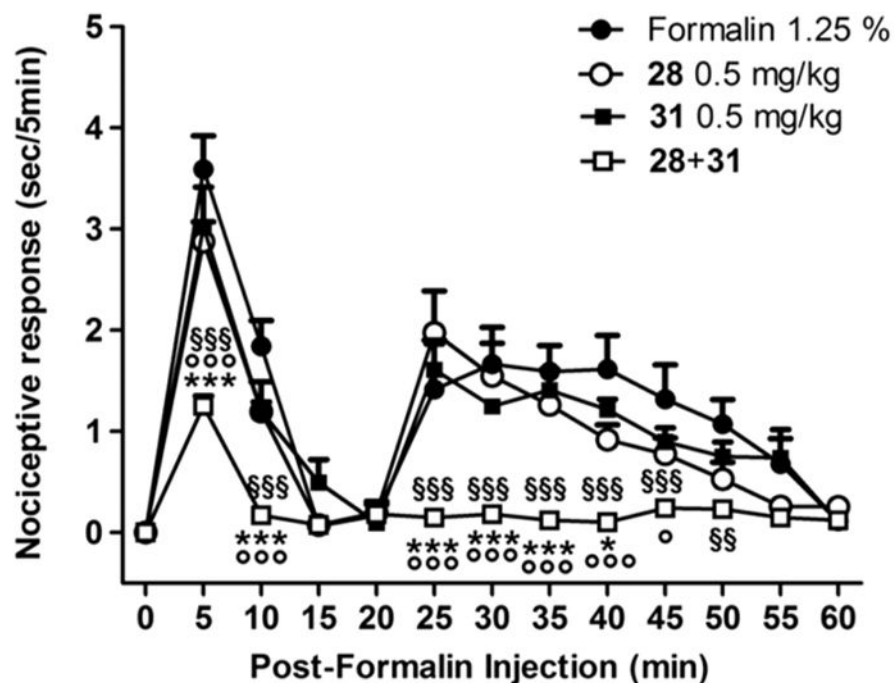


Figure 6. Effect of subcutaneous formalin (1.25%, 30 μ L) injections into the hind paw of mice on the time course of the nociceptive behaviors. Formalin was injected 10 min after the systemic administration of vehicle (0.9% NaCl, ip) or drugs. Effects of the systemic administration of **28** (0.5 mg/kg, ip) and **31** (0.5 mg/kg, ip) alone or in combination. Recording of nocifensive behavior began immediately after the injection of formalin (time 0) and was continued for 60 min. Each point represents the total time of the nociceptive responses (mean (SEM) of 8 mice per group, measured every 5 min. § indicates significant differences versus vehicle, * indicates significant differences versus **28** (0.5 mg/kg), and ○ indicates significant differences versus **31** (0.5 mg/kg). $P < 0.05$ was considered statistically significant.

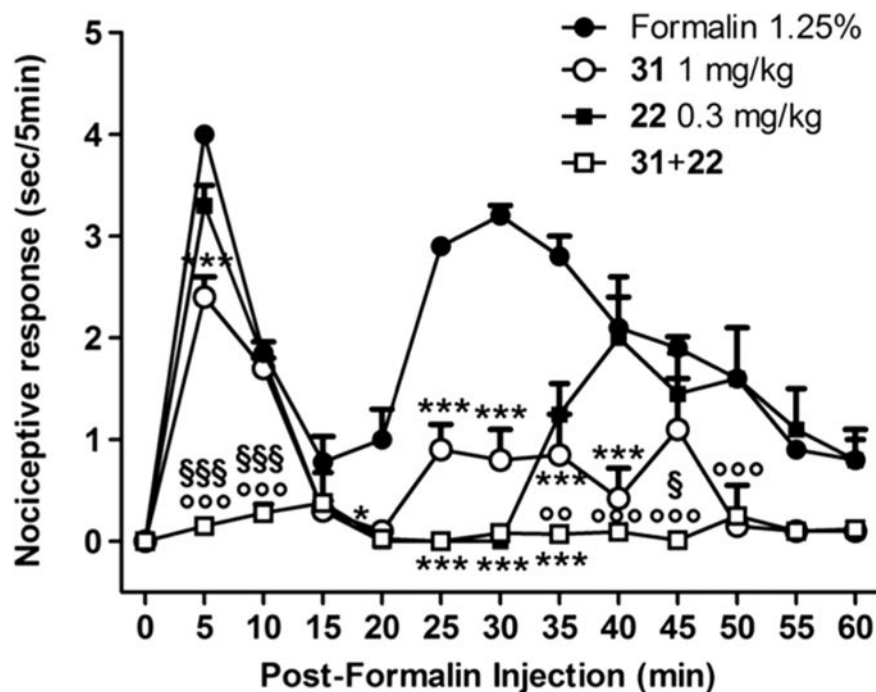
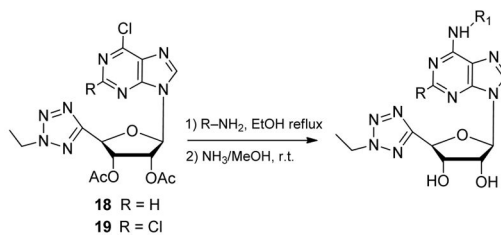


Figure 7.

Effect of subcutaneous formalin (1.25%, 30 μ L) injections into the hind paw of mice on the time course of the nociceptive behaviors. Formalin was injected 10 min after the systemic administration of vehicle (0.9% NaCl, ip) or drugs. Effects of the systemic administration of **22** (0.3 mg/kg, ip) and **31** (1 mg/kg, ip) alone or in combination. Recording of nocifensive behavior began immediately after the injection of formalin (time 0) and was continued for 60 min. Each point represents the total time of the nociceptive responses (mean (SEM) of 8 mice per group, measured every 5 min). * indicates significant differences versus vehicle, ○ indicates significant differences versus **22** (0.3 mg/kg), and § indicates significant differences versus **31** (1 mg/kg). $P < 0.05$ was considered statistically significant.

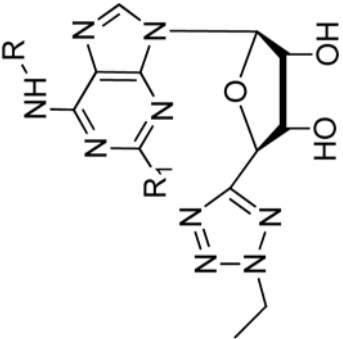


- 1 R = H, R₁ = cyclopropyl
- 2 R = Cl, R₁ = cyclopropyl
- 3 R = H, R₁ = cyclopropylmethyl
- 4 R = Cl, R₁ = cyclopropylmethyl
- 5 R = H, R₁ = furyl-2-methyl
- 6 R = Cl, R₁ = furyl-2-methyl
- 7 R = H, R₁ = thienyl-2-methyl
- 8 R = Cl, R₁ = thienyl-2-methyl
- 9 R = H, R₁ = 3-fluoro-benzyl
- 10 R = Cl, R₁ = 3-fluoro-benzyl
- 11 R = H, R₁ = 3-chloro-benzyl
- 12 R = Cl, R₁ = 3-chloro-benzyl
- 13 R = H, R₁ = 3-bromo-benzyl
- 14 R = Cl, R₁ = 3-bromo-benzyl
- 15 R = H, R₁ = 3-iodo-benzyl
- 16 R = H, R₁ = 2-fluoro-4-chloro-benzyl
- 17 R = Cl, R₁ = 2-fluoro-4-chloro-benzyl

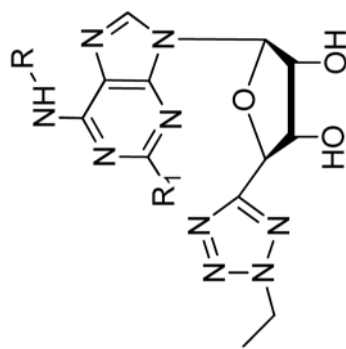
Scheme 1.
Synthesis of Target Compounds 1–17

Table 1

Binding Affinity of 5'-C-Ethyltetrazolyladenosine Derivatives



compd	R	R ₁	K _i (nM) ^a		
			A ₁ ^b	A _{2A} ^c	A ₃ ^d
1	cyclopropyl	H	0.864 (0.464–1.61)	146 (133–161)	0.875 (0.85–0.90)
2	cyclopropyl	Cl	0.538 (0.453–0.640)	274 (235–318)	0.461 (0.342–0.622)
3	cyclopropylmethyl	H	0.438 (0.361–0.523)	112 (81.4–153)	0.575 (0.55–0.60)
4	cyclopropylmethyl	Cl	0.454 (0.431–0.478)	329 (288–377)	0.313 (0.251–0.391)
5	furyl-2-methyl	H	10.7 (9.5–12.0)	342 (229–512)	4.85 (3.58–6.57)
6	furyl-2-methyl	Cl	7.64 (5.75–10.1)	663 (599–733)	1.31 (1.02–1.68)
7	thienyl-2-methyl	H	3.53 (2.82–12.0)	98.4 (58.5–165)	2.35 (1.72–3.22)
8	thienyl-2-methyl	Cl	6.02 (4.44–8.16)	286 (253–323)	1.59 (1.49–1.68)
9	3-fluorobenzyl	H	3.73 (2.95–4.71)	74.0 (48.6–113)	1.20 (1.03–1.4)
10	3-fluorobenzyl	Cl	6.04 (4.38–8.32)	242 (197–297)	0.806 (0.661–0.983)
11	3-chlorobenzyl	H	1.41 (1.07–1.85)	29.8 (25.3–35.1)	0.386 (0.324–0.459)
12	3-chlorobenzyl	Cl	2.71 (2.50–2.93)	110 (93.0–129)	0.387 (0.276–0.544)
13	3-bromobenzyl	H	0.950 (0.535–1.68)	24.5 (14.0–42.9)	0.393 (0.347–0.445)
14	3-bromo-benzyl	Cl	1.79 (1.64–1.96)	58.2 (47.8–71.0)	0.345 (0.231–0.514)
15	3-iodobenzyl	H	0.768 (0.720–0.820)	16.8 (13.0–21.8)	0.532 (0.282–1.0)
16	2-fluoro-4-chlorobenzyl	H	4.28 (4.08–4.48)	252 (205–310)	4.67 (3.73–5.85)



compd	R	K_i (nM) ^a			
		R ₁	A ₁ ^b	A _{2A} ^c	A ₃ ^d
17	2-fluoro-4-chlorobenzyl	Cl	17.6 (14.8–21.0)	881 (783–990)	5.17 (4.31–6.20)
20^e	H	H	0.919 (0.716–1.18)	8.12 (6.01–11.0)	3.86 (3.49–4.28)
21^e	H	Cl	0.966 (0.770–1.21)	20.7 (16.9–25.3)	1.80 (1.42–2.29)
22^e	CH ₃	H	3.56 (3.02–4.19)	778 (685–883)	0.478 (0.421–0.541)
23^e	CH ₃	Cl	8.59 (8.11–9.10)	3350 (2920–3840)	0.429 (0.361–0.509)
24^e	2-fluoro-4-chlorophenyl	H	0.432 (0.330–0.565)	77.5 (69.4–86.6)	2.61 (1.84–3.71)
25^e	2-fluoro-4-chlorophenyl	Cl	1.67 (1.42–1.97)	223 (206–241)	4.71 (3.49–6.36)
26^e	3-iodobenzyl	Cl	2.39 (2.18–2.62)	108 (68.5–171)	0.588 (0.540–0.641)

^a K_i values are given in nM with 95% confidence intervals in parentheses.

^b Displacement of specific [³H]2-chloro-*N*⁶-cyclopentyladenosine (**32**, CCPA)⁴³ binding in CHO cells transfected with the recombinant hA₁AR.

^c Displacement of specific [³H]adenosine-5'-*N*-ethyluronamide (**33**, NECA)⁴¹ binding in CHO cells transfected with recombinant hA_{2A}AR.

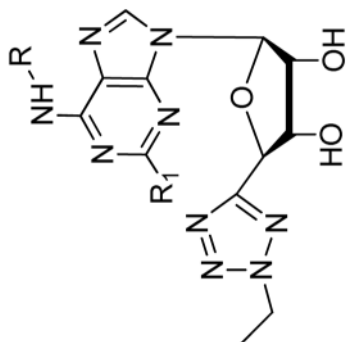
^d Displacement of specific [³H]2-(1-hexynyl)-*N*⁶-methyladenosine (**34**, HEMADO) binding in CHO cells transfected with recombinant hA₃AR.⁴⁰

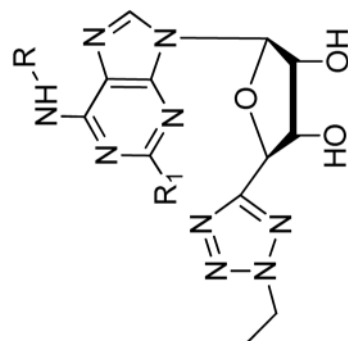
^e Data from Petrelli et al.⁷

Table 2

EC₅₀ Values for Adenylyl Cyclase Activation (A_{2A} and A_{2B}) or Inhibition (A₁ and A₃)^a

compd	R	EC ₅₀ (nM)				
		R ₁	A ₁	A _{2A}	A _{2B}	A ₃
1	cyclopropyl	H	7.66 (4.71–12.5)	21.6 (20.1–23.2)	222 (147–336) (p _{act} 86%)	5.40 (3.16–9.22)
2	cyclopropyl	Cl	7.21 (6.89–7.54)	21.5 (16.6–27.9)	677 (556–824)	14.1 (10.4–19.10)
3	cyclopropylmethyl	H	7.73 (5.57–10.7)	16.6 (15.3–17.9)	637 (500–813) (p _{act} 81%)	3.53 (1.21–7.10)
4	cyclopropylmethyl	Cl	7.21 (5.64–9.21)	28.6 (24.7–33.1)	1961 (1527–2518)	14.4 (8.95–17.0)
5	furyl-2-methyl	H	552 (361–844)	54.3 (38.5–76.6)	1930 (1140–3270)	125 (83.8–185)
6	furyl-2-methyl	Cl	341 (259–449)	60.2 (57.4–63.1)	2570 (1960–3370)	52.4 (48.5–56.5)
7	thienyl-2-methyl	H	208 (159–273)	14.7 (11.2–19.3)	527 (298–929)	59.7 (32.5–110)
8	thienyl-2-methyl	Cl	222 (199–248)	38.4 (31.6–46.7)	2140 (1340–3430)	44.7 (35.6–56.1)
9	3-fluoro-benzyl	H	147 (95.6–227)	14.4 (12.8–16.2)	1100 (682–1760) (p _{act} 86%)	12.5 (7.23–21.8)
10	3-fluorobenzyl	Cl	239 (142–400)	31.3 (24.2–40.6)	2230 (2020–2450)	31.5 (24.6–40.3)
11	3-chlorobenzyl	H	58.5 (50.2–68.3)	6.71 (6.28–7.17)	592 (366–957)	2.20 (1.26–3.84)
12	3-chlorobenzyl	Cl	116 (90.3–148)	16.0 (12.4–20.6)	2390 (1640–3500)	7.61 (6.47–8.95)
13	3-bromobenzyl	H	45.1 (34.9–58.2)	4.46 (4.17–4.78)	408 (288–576)	2.07 (0.993–4.30)
14	3-bromobenzyl	Cl	72.8 (50.2–106)	13.3 (10.8–16.4)	1650 (1360–1990)	9.64 (5.83–15.9)
15	3-iodobenzyl	H	27.4 (22.0–34.1) (p _{act} 87%)	2.87 (1.67–4.92)	235 (174–319)	2.38 (1.38–4.12)
16	2-fluoro-4-chlorobenzyl	H	230 (189–280)	40.7 (38.9–42.6)	1290 (739–2260)	25.4 (20.1–32.1)



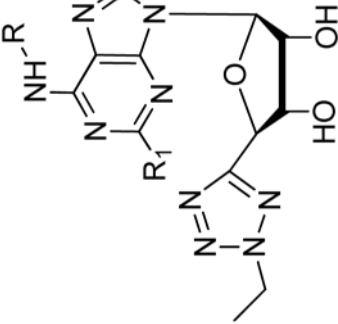


compd	R	EC ₅₀ (nM)				
		R ₁	A _{2A}	A _{2B}	A ₃	
17	2-fluoro-4-chlorobenzyl	Cl	539 (359–809)	96.5 (85.5–109)	>30 000	105 (95.6–116)
20^b	H	H	26.3 (20.8–33.3)	2.36 (2.00–2.78)	347 (266–454)	93.6 (79.7–110)
21^b	H	Cl	19.8 (14.3–27.5)	3.84 (3.32–4.44)	542 (340–865)	31.7 (23.2–43.2)
22^b	CH ₃	H	97.2 (84.4–112)	1710 (1150–2530)	1480 (923–2390)	6.38 (5.03–8.07)
23^b	CH ₃	Cl	250 (204–307)	238 (206–274)	3510 (2290–5360) (<i>pag 75%</i>)	7.69 (6.34–9.32)
24^b	2-fluoro-4-chlorophenyl	H	10.2 (9.48–11.1)	8.40 (7.41–9.53)	530 (314–896)	33.9 (21.1–54.5)
25^b	2-fluoro-4-chlorophenyl	Cl	64.8 (47.9–87.8)	28.8 (20.8–39.9)	1110 (888–1400)	37.0 (27.1–50.7)
26^b	3-iodobenzyl	Cl	64.9 (54.2–77.8)	9.04 (6.37–12.8) (<i>pag 75%</i>)	834 (563–1230) (<i>pag 76%</i>)	13.3 (6.72–26.5)

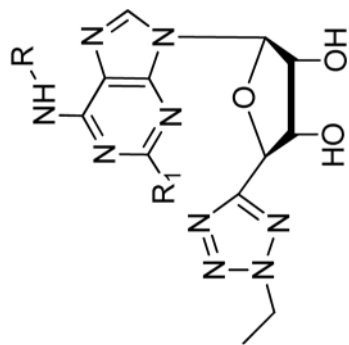
^a All tested compounds are full agonists at the hA₁, hA_{2A}, and hA_{2B} receptor (efficacy 90% unless stated otherwise). All tested compounds are antagonists at the hA₃ receptor. *pag*, partial agonist (% efficacy).

^b Data from Petrelli et al.⁷

Table 3

Binding Affinity of 5'-C-Ethyltetrazolyladenosine Derivatives at Rat and Human A₃AR


compd	R	R ₁	K _i ^a (nM)		
			rA ₃ (all agonists) ^b	hA ₃ (all antagonists) ^c	rA ₃ /hA ₃
1	cyclopropyl	H	66.0 (39.3–111)	0.875 (0.85–0.90)	76
3	cyclopropylmethyl	H	65.2 (51.7–82.0)	0.575 (0.55–0.60)	110
5	furyl-2-methyl	H	33.1 (22.7–48.3)	4.85 (3.58–6.57)	6.8
7	thienyl-2-methyl	H	10.1 (8.46–12.1)	2.35 (1.72–3.22)	4.3
9	3-fluorobenzyl	H	9.26 (8.64–9.93)	1.20 (1.03–1.40)	7.7
11	3-chlorobenzyl	H	2.69 (1.91–3.79)	0.386 (0.324–0.459)	6.9
13	3-bromobenzyl	H	4.11 (2.32–7.24)	0.393 (0.347–0.445)	10
15	3-iodobenzyl	H	6.10 (3.52–10.6)	0.532 (0.282–1.0)	12
16	2-fluoro-4-chlorobenzyl	H	22.6 (20.9–24.4)	4.67 (3.73–5.85)	4.8
20	H	H	228 (139–374)	3.86 (3.49–4.28) ^d	59
21	H	Cl	212 (151–297)	1.80 (1.42–2.29) ^d	120
22	CH ₃	H	484 (442–529)	0.478 (0.421–0.541) ^d	1000
23	CH ₃	Cl	600 (518–695)	0.429 (0.361–0.509) ^d	1400
24	2-fluoro-4-chlorophenyl	H	21.4 (15.0–30.4)	2.61 (1.84–3.71) ^d	8.1



K_i^a (nM)

compd	R	R ₁	rA ₃ (all agonists) ^b	hA ₃ (all antagonists) ^c	rA ₃ /hA ₃
26	3-iodobenzyl	Cl	2.53 (1.66–3.85)	0.588 (0.540–0.641) ^d	4.3

^a K_i values are given in nM with 95% confidence intervals in parentheses.

^b Displacement of specific [³H]33 (30 nM) binding in CHO cells transfected with recombinant rA₃AR.

^c Displacement of specific [³H]34 (1 nM) binding in CHO cells transfected with recombinant hA₃AR.

^d Data from Petrelli et al.⁷

Table 4

Selectivity Ratios for hAR Binding Affinities^a

compd	R	R ₁	selectivity		
			A _{2A} /A ₁	A _{2A} /A ₃	A ₃ /A ₁
1	cyclopropyl	H	170	168	1.0
2	cyclopropyl	Cl	509	596	0.86
3	cyclopropylmethyl	H	256	196	1.3
4	cyclopropylmethyl	Cl	725	1097	0.66
5	furyl-2-methyl	H	32	70	0.45
6	furyl-2-methyl	Cl	87	506	0.17
7	thienyl-2-methyl	H	28	42	0.67
8	thienyl-2-methyl	Cl	47	180	0.26
9	3-fluorobenzyl	H	20	62	0.32
10	3-fluorobenzyl	Cl	40	299	0.13
11	3-chlorobenzyl	H	21	77	0.27
12	3-chlorobenzyl	Cl	40	282	0.14
13	3-bromobenzyl	H	25	61	0.4
14	3-bromobenzyl	Cl	32	171	0.19
15	3-iodo-benzyl	H	22	32	0.69
16	2-fluoro-4-chlorobenzyl	H	59	54	1.09
17	2-fluoro-4-chlorobenzyl	Cl	50	170	0.29
20 ^b	H	H	9	2	4
21 ^b	H	Cl	21	12	2
22 ^b	CH ₃	H	218	1630	0.13
23 ^b	CH ₃	Cl	390	7800	0.05
24 ^b	2-fluoro-4-chlorophenyl	H	180	30	6
25 ^b	2-fluoro-4-chlorophenyl	Cl	130	47	3
26 ^b	3-iodobenzyl	Cl	45	180	0.25

^a Values in bold mark compounds with selectivities of 30 for both A₁ and A₃ vs A_{2A}. A₁ vs A₃ selectivity is 10 for all compounds.

Data from Petrelli et al.⁷

Author Manuscript

Author Manuscript

Author Manuscript

Author Manuscript